# Myeloid derived Oncostatin M reprogrammes cancer-associated fibroblasts and tumour cells promoting breast cancer progression.

Angela M. Araujo[1], Andrea Abaurrea[1], Peio Azcoaga[1], Joanna I. López-Velazco[1], Ricardo Rezola[2], Iñaki Osorio-Querejeta[1], Fátima Valdés-Mora[3,4], Juana M. Flores[5], Liam Jenkins[6], Patricia Fernández-Nogueira[7], Nicola Ferrari[8], Natalia Martín-Martín[9,10], Alexandar Tzankov[11], Serenella Eppenberger-Castori[11], Isabel Alvarez-Lopez[1,2], Ander Urruticoechea[1,2], Paloma Bragado[12], Nicholas Coleman[13], Arkaitz Carracedo[9,10,14,15], David Gallego-Ortega[3,16] , Fernando Calvo[8,17], Clare M. Isacke[6], Maria M. Caffarel[1,14*#], Charles H. Lawrie[1,14,18,#]

[1]Biodonostia Health Research Institute, San Sebastian, Spain. [2]Gipuzkoa Cancer Unit, OSI Donostialdea - Onkologikoa Foundation, San Sebastian, Spain. [3]Cancer Epigenetic Biology and Therapeutics Laboratory, Children's Cancer Institute, Sydney, Australia. [4]St. Vincent's Clinical School, UNSW, Sydney, Australia. [5]Department of Animal Medicine and Surgery, Complutense University of Madrid, Madrid, Spain. [6]The Breast Cancer Now Toby Robins Research Centre, The Institute of Cancer Research, London, United Kingdom. [7]Department of Biochemistry and Molecular Biomedicine, University of Barcelona; Institute of Biomedicine, University of Barcelona (IBUB), Barcelona, Spain. [8]Tumour Microenvironment Lab, The Institute of Cancer Research, London, United Kingdom. [9]Center for Cooperative Research in Biosciences (CIC bioGUNE), Basque Research and Technology Alliance (BRTA), Bizkaia Technology Park, Derio, Spain. [10]CIBERONC (Centro de Investigación Biomédica en Red de Cáncer), Madrid, Spain. [11]Institute of Medical Genetics and Pathology, University Hospital, Basel, Switzerland. [12]Department of Biochemistry and Molecular Biology, Faculty of Pharmacy, Complutense

University of Madrid, Health Research Institute of the Hospital Clínico San Carlos, Madrid, Spain. [13]Department of Pathology, University of Cambridge, Cambridge, United Kingdom. [14]IKERBASQUE, Basque Foundation for Science, Bilbao, Spain. [15]Department of Biochemistry and Molecular Biology, Faculty of Science and Technology, University of the Basque Country, Bilbao, Spain. [16]Tumour Development Laboratory, The Kinghorn Cancer Centre, Garvan Institute of Medical Research, Sydney, Australia. [17]Instituto de Biomedicina y Biotecnología de Cantabria, Santander, Spain. [18]Radcliffe Department of Medicine, University of Oxford, Oxford, United Kingdom.

***Correspondence to**: Dr. Maria M. Caffarel, Biodonostia Health Research Institute, San Sebastian, 20014, Spain and IKERBASQUE, Basque Foundation for Science, Bilbao, 48013, Spain, Email: maria.caffarel@biodonostia.org, Tel: +34943328193.

**# Co-last authors**

**Abstract**

Cytokines are key players in inflammation, a process associated with tumour initiation, angiogenesis and metastasis. However, the interplay between inflammation and other cell types in the tumour microenvironment is not well understood. Here we show that the IL6-related proinflammatory cytokine Oncostatin M (OSM) is a central node for multicellular interactions. Myeloid-derived OSM reprogrammes cancer-associated fibroblasts (CAFs) and cancer cells, promoting breast cancer progression. In addition, OSM induces, in both cell types, the secretion of inflammatory cytokines and chemokines, which in turn reinforce myeloid tumour infiltration. OSM is increased in cancer stroma and is associated with poor prognosis in multiple cancer types. Oncostatin M receptor (OSMR) deletion in stroma and in a multistage breast cancer mouse model delays tumour onset, tumour growth and reduces metastatic burden. Our results reveal an unprecedented tumour-promoting paracrine OSM:OSMR signalling crosstalk encompassing myeloid cells, CAFs and tumour cells, thus encouraging therapeutic strategies aimed at targeting this oncogenic axis in breast cancer.

**Introduction**

Tumour-promoting inflammation is a hallmark of cancer that influences all stages of tumour progression[1]. Therapies aimed at modulating inflammatory responses in the tumour microenvironment have been of great interest in recent years[2]. The tumour microenvironment (TME) is composed of several different cell types (i.e. fibroblasts, adipocytes, endothelial and infiltrating immune cells) with complex interactions. Cancer cells are constantly communicating with the surrounding stroma and they hijack physiological interactions to overcome immune system surveillance and promote cancer progression[3]. Cancer-associated fibroblasts (CAFs) are a key cell population in the TME[4]. Apart from their very well-known functions in matrix deposition and extracellular matrix remodelling, CAFs have recently been

shown to interact with the immune system by responding to and secreting chemokines and cytokines[4].

However, the interplay between inflammation, cancer cells and other cell types in the TME is not well understood. Cytokines act as central signalling nodes for multicellular interactions. They are very important in cancer-related inflammatory processes as they are responsible for controlling cell recruitment and modulating immune cell responses in the TME[5]. Here we show that the pro-inflammatory cytokine Oncostatin M (OSM) is a key player in mediating the crosstalk between immune cells, CAFs and cancer cells; and that these immune-stromal-cancer cell interactions favour breast cancer progression and metastasis.

OSM belongs to the IL6 family, which is considered one of the most important cytokine families in the process of tumorigenesis and metastasis[6]. IL6, in particular, is one of the best characterized tumour-promoting cytokines and it is highly up-regulated in many cancers[7]. OSM was first described as an anti-tumoural cytokine due to its anti-proliferative effect in melanoma and other cancer cells[8]. However, in recent years, OSM has been associated with tumour progression as it induces EMT transition, cancer stem-like features, cell migration and metastasis in animal and cellular models[9,10]. High oncostatin M receptor (OSMR) expression correlates with decreased survival in clinical samples of glioblastoma, breast and cervical cancer[11–13]. However, the information regarding the role of OSM signalling in the TME is scarce, restricted to reports describing altered mRNA expression in this compartment[14,15] and a role for OSM in macrophage M2 polarization[16].

By using samples from primary breast tumours, transgenic and orthotopic mouse models of breast cancer, single-cell analysis and *in vitro* cultures we demonstrate that OSM is a central node for multicellular interactions within the breast TME. OSM is mainly produced by tumour-infiltrating myeloid cells, while its receptor OSMR is highly expressed by CAFs and cancer cells. OSMR activation in CAFs and cancer cells reprogrammes CAF phenotype and promotes the

secretion of inflammatory chemokines, generating a positive feedforward loop that leads to sustained tumour inflammation and consequent breast cancer progression. Importantly, OSMR depletion in both cancer cells and TME, or only in the TME, decreased tumour onset and tumour growth, and reduced metastasis.

This work reveals a clear paracrine signalling between the immune system, CAFs and tumour cells supporting the notion that targeting OSM:OSMR interactions is a potential therapeutic strategy to inhibit tumour-promoting inflammation and breast cancer progression. Of interest, targeting IL6 to block chronic inflammation in cancer is problematic and anti-IL6 drugs have not yielded significant results against solid tumours in clinical trials[17,18]. It may be worth exploring therapeutic targeting of OSM signalling as an alternative. Importantly, humanized antibodies against OSM are being tested in clinical trials for the treatment of inflammatory diseases and have shown to be safe and well tolerated[19].

## Results

### Oncostatin M (OSM) expression associates with poor survival in breast cancer.

Although breast cancer is not directly associated with persistent infections or extrinsic chronic inflammation, tumour-elicited inflammation is increasingly being recognized as an important contributor to breast cancer progression[20]. To determine the relevance of the pro-inflammatory OSM signalling in breast cancer prognosis, we performed immunohistochemistry (IHC) in 141 samples of early breast cancer included in 3 tissue microarrays (TMAs) and observed that high OSM protein levels were associated with decreased overall survival (P=0.029) (Fig. 1a,b). In addition, OSM expression was significantly increased in the cases with high inflammation, assessed by the pathologist as infiltration of inflammatory cells from all lymphoid and myeloid subtypes (Fig. 1b,c). We observed that OSM was mainly expressed by

myeloid-like cells as determined by their larger size and more irregular shape (Fig. 1b). Lymphoid cells, characterized by being smaller and round and by having a round nucleus with little cytoplasm, showed very low or negative OSM expression (Fig. 1b).

We confirmed the association between OSM expression and poor survival in published gene expression profiles of breast cancer, observing that increased OSM mRNA levels associated with decreased disease-free survival (Fig. 1d and Extended Data Fig.1a) in the Metabric[21] and Wang[22] datasets. By analysing TCGA data by Kaplan-Meier Plotter[23] we observed that high OSM levels were significantly associated with worse overall survival in a large number of cancer types (Extended Data Fig. 1b). These data indicate that OSM associates with poor survival and inflammation in breast cancer and that it could also be relevant in other tumour types.

**Deletion of Oncostatin M Receptor (OSMR) in the pre-clinical model MMTV-PyMT impairs tumour progression.**

As OSM is mainly secreted by immune cells in the breast cancer microenvironment (Fig. 1b), we decided to use an immunocompetent mouse model to test the relevance of the OSMR signalling pathway in breast cancer progression. We crossed Oncostatin M Receptor (OSMR) deficient mice with MMTV-PyMT as illustrated by the experiment scheme in Fig. 2a. The MMTV-PyMT mouse is a widely used mouse model to study breast cancer progression with an intrinsic tumour microenvironment and immune system[24]. It expresses Polyoma Virus Middle T antigen under the control of the mouse mammary tumour virus promoter/enhancer and develops, from 5-7 weeks of age, spontaneous breast tumours, which metastasize to the lungs within 14 weeks or less. This transgenic model progresses through four distinctly identifiable stages of tumour progression (from benign or *in situ* lesions to invasive carcinomas) and mimics well the progression of human breast cancer[24]. MMTV-PyMT: OSMR KO females showed a significant delay in tumour onset compared to their WT and HET littermates (Fig. 2b

and Extended Data Fig. 2a,b). In addition, OSMR depletion delayed tumour growth and significantly reduced tumour burden at 14 weeks of age, when WT and HET animals reached a humane endpoint (Fig. 2c,d). Whole mount analysis of mammary glands at 9 week of age revealed reduction of preneoplastic lesions in MMTV-PyMT: OSMR KO compared to control mice (Extended Data Fig. 2c). At 14 weeks of age, most of the control animals (19 out of 21 for WT; and 17 out of 20 for HET) harboured tumours that were malignant carcinomas with necrotic areas, while the KO group contained 7 animals with carcinomas, 7 with pre-malignant adenomas/ mammary intraepithelial neoplasia (MIN) and 1 mouse showed no tumours (Fig. 2e and Extended Data Fig. 2d, P value = 0,007 for Chi Square test comparing malignant lesions versus pre-malignant lesions or no lesions). Interestingly, when compared to their controls, tumours in OSMR-deficient mice showed decreased levels of the extracellular matrix protein fibronectin, predominantly produced by CAFs[25] (Fig 2f), increased levels of apoptosis, but similar degree of proliferation (Extended Data Fig. 2e). Finally, OSMR deficiency produced a remarkable reduction in the percentage of animals with lung metastases. While 86 and 65 % of WT and HET mice, respectively, developed lung micro or macrometastasis, 80 % of KO mice remained metastasis free (Fig. 2g,h). In summary, our data in the MMTV-PyMT model demonstrate that OSMR signalling is an important contributor of breast cancer progression.

**The OSM:OSMR signalling module exhibits a distinct microenvironment-restricted expression.**

We performed single cell RNA-seq analysis of mammary tumours from the MMTV-PyMT model to decipher which cells were responsible to produce OSM and to express OSMR in the breast cancer context. Our data indicate that the ligand OSM is almost exclusively expressed by the myeloid cell population (as suggested by the OSM staining in Fig. 1b), while the receptor OSMR is mainly expressed by the fibroblasts and some of the cancer epithelial clusters (Fig. 3a-c). The pattern of expression of OSM:OSMR differs from the one observed for other cytokine-receptor

pairs of the same family such as IL6:IL6R (Il6ra) and LIF:LIFR (Fig. 3b,c), supporting that OSM exerts distinct and unique functions from other members of the family[26]. Il6st (GP130) is the common subunit receptor for OSM, IL6, LIF and other cytokines of the family and is ubiquitously expressed (Fig. 3b,c), being the expression of the other receptor subunits more restricted and tightly regulated. RT-qPCR analysis of FACS-sorted breast TS1 orthotopic tumours[27] confirmed expression of OSM in the CD45+ CD11b+ myeloid population and expression of OSMR in fibroblasts and cancer cells (Fig. 3d,e and Extended Data Fig. 3a). Similar results were obtained when analysing FACS sorted populations of MMTV-PyMT tumours (Extended Data Fig. 3b).

An identical pattern of OSM:OSMR expression is maintained in the human setting, as demonstrated by RT-qPCR quantification in a large panel of human cell lines and analysis of RNA-seq data from the Human Protein Atlas[28] (Fig. 3f and Extended Data Fig. 3c,d). OSM mRNA could not be detected in breast cancer cell lines and fibroblasts by RT-qPCR (Extended Data Fig.3c and data not shown). It was only expressed in undifferentiated and macrophage-like differentiated HL-60 cells[29] (Extended Data Fig.3c) and in lymphoid and myeloid cell lines (Extended Data Fig. 3d). Conversely, OSMR was only detected by RT-qPCR in breast cancer cells and fibroblasts, showing significantly higher expression in fibroblasts compared to epithelial cells (Fig. 3f and Extended Data Fig. 3c). Analysis of a battery of human cell lines[28] confirmed expression of OSMR only in epithelial, endothelial and fibroblast cell lines and not in immune cell lines (Extended Data Fig. 3d).

To prove the relevance of our previous findings in human cancer clinical data, we used the xCell[30] and TIMER[31] web resources to analyse the association between OSM and OSMR expression and TME composition in two different clinical breast cancer datasets[32,33]. xCell analysis showed that OSMR mRNA expression significantly correlates with fibroblast enrichment in human breast cancer, while OSM mRNA levels show the most significant

associations with macrophage M2-like and common myeloid progenitor signatures (Fig. 4a). The OSM and OSMR correlations with fibroblasts and myeloid cell infiltration respectively, were validated by TIMER in a different clinical dataset (Extended Fig.4a). This analysis also showed that OSM and OSMR mRNA expression inversely correlated with tumour cell purity. In line with these results, OSM and OSMR mRNA levels were found to be elevated in breast cancer stroma compared to the epithelial compartment in a different dataset (Fig. 4b). Moreover, both OSM and OSMR are increased in human breast cancer stroma compared to healthy stroma (Fig. 4c). A similar pattern of OSM:OSMR expression was observed in other cancer types including ovarian and colorectal cancer (Extended data Fig. 4b,c). Altogether, our data reveal that OSM and OSMR are stroma-expressed molecules, and point to paracrine OSM:OSMR signalling in cancer, as ligand and receptor are expressed by different cell types in the tumour microenvironment.

**Stromal OSMR deletion hampers tumour progression and aggressiveness.**

To test the hypothesis that stromal OSM:OSMR signalling contributed to breast cancer progression we injected TS1 cells, derived from a MMTV-PyMT tumour[27], orthotopically into the mammary gland of syngeneic OSMR deficient (KO) and wild-type (WT) control mice (Fig. 4d). This model allows the assessment of the contribution of stromal OSMR signalling to cancer progression as OSMR is only depleted in cells of the tumour microenvironment while TS1 cancer cells express OSMR that can be activated by host-derived OSM (Extended Data Fig. 4d,e). Depletion of OSMR in the tumour microenvironment resulted in delayed tumour onset and tumour growth (Fig. 4e-g and Extended Data Fig. 4e) confirming that stromal OSMR signalling contributes to cancer progression.

**OSM activates cancer-associated fibroblasts *in vitro* and *in vivo*, promoting tumour progression.**

As we previously observed that fibroblasts were the cell population with higher levels of OSMR within the stroma (Fig. 3), we performed complementary *in vitro* and *in vivo* experiments to assess the effect of OSMR activation in mammary cancer-associated and normal fibroblasts derived from human breast tumours and reduction mammoplasty surgeries[34], respectively. The ability to remodel the extracellular matrix is a hallmark of CAFs[25]. Importantly, OSM treatment enhanced the capacity of CAFs (CAF-173 and CAF-318) to contract collagen matrices and, interestingly, the effect was not observed in non-cancerous skin and breast fibroblasts (HS27 and RMF-31, respectively) (Fig. 5a). To further investigate the role of OSM in potentiating CAFs activation, we selected RMF-31 to be used as a model of normal breast fibroblasts and CAF-173 as a model of CAFs. In accordance with the contractility experiments, OSM promoted the growth of 3D CAF spheroids while it did not affect normal mammary fibroblasts 3D spheroids (Fig. 5b). Similarly, OSM induced the expression of classical CAF markers such as FAP, POSTN, VEGF and IL6[25], only in CAF-173 CAFs, and not in normal RMF-31 fibroblasts (Fig. 5c). Of interest, OSMR was similarly expressed in normal and cancer fibroblasts (Fig. 3f) and the pathway was functional in both CAFs and normal fibroblasts, as suggested by OSM induction of OSMR expression in both cell lines and phosphorylation of STAT3 in CAF-173 (Extended Data Fig. 5a,b), classical hallmarks of OSMR activation[35]. Gene set enrichment analysis (GSEA) of transcriptomic data of CAF-173 treated with OSM or vehicle, showed that OSM induced signatures related to JAK-STAT3 signalling and fibroblast activation (Fig. 5d and Extended Data Fig. 5c). A transcriptional signature composed by the top differentially expressed genes by OSM in CAF-173 was enriched in the breast cancer stroma GSE9014 dataset compared to normal stroma (Extended Data Fig. 5d). Importantly, the top 4 genes induced by OSM in CAF-173 (SERPINB4, THBS1, RARRES1 and TNC, Extended Data Fig. 5e) are associated with decreased recurrence-free survival in breast cancer patients (Fig. 5e). In addition, THBS1, RARRES1 and TNC levels correlate with OSM and OSMR expression in breast cancer clinical samples (Extended Data Fig. 5f). These results indicate that OSM induces in CAFs

the expression of pro-malignant genes, including fibroblast activation markers and genes associated with JAK-STAT3 signalling.

In order to test if the OSM-induced changes in CAFs contributed to breast cancer progression *in vivo*, we pre-treated CAF-173 CAFs with OSM or PBS (Control) for 4 days *in vitro* and orthotopically co-injected them with MDA-MB-231 breast cancer cells into Athymic Nude-Foxn1nu mice as described in the experiment timeline in Fig. 5f. Activation of fibroblasts by OSM promoted tumour growth (Fig. 5g,h) and exhibited a trend to increase lung colonization (Fig. 5i), assessed by qPCR analysis of human Alu DNA sequences in the lungs[36]. Conversely, OSMR downregulation by shRNA in CAF-173 delayed tumour onset and tumour growth at early stages when co-injected with MDA-MB-231 breast cancer cells ectopically expressing human OSM (Extended Data Fig. 5g-j). In addition, downregulation of OSMR in CAFs decreased IL6 expression in tumours, suggesting that OSM is inducing the expression of similar targets *in vivo* (Extended Data Fig.5k). Moreover, the tumours with OSMR silencing in CAFs showed reduced levels of GFP (Extended Data Fig. 5k), suggesting reduced levels of CAFs in this experimental group, probably due to impaired CAF proliferation upon OSMR reduction, in line with the increased size of CAF spheres observed after OSMR activation (Fig. 5b). Together, our data prove that OSM:OSMR signalling activates CAFs and that this contributes to cancer progression.

**OSM:OSMR signalling in CAFs and cancer cells induces cytokine secretion and myeloid cell recruitment, establishing a positive feedback loop.**

In an attempt to understand how OSMR activation in tumours was inducing malignancy we analysed transcriptomic data of CAFs (CAF-173) and breast cancer cells (MDA-MB-231) activated with OSM. Microarray data indicated that pathways related to leukocyte recruitment and neutrophil degranulation were significantly enriched upon OSM activation (Fig. 6a and Extended Data Fig. 6a). In addition, GSEA analysis showed that the inflammatory response

hallmark signature from Molecular Signatures Database (MsigDB)[37] was enriched in both CAF-173 and MDA-MB-231 activated with OSM (Fig. 6b). These data suggested that, upon OSMR activation by OSM, both CAFs and cancer cells could be involved in shaping the tumour microenvironment by recruiting leukocytes to the tumour site. Analysis of a panel of 31 chemokines by antibody array showed that OSM induced expression of important chemoattractants (Fig. 6c and Extended Data Fig. 6b). Some of these factors were exclusive of CAFs (mainly CXCL10 and CXCL12), others of cancer cells (mainly CXCL7 and CCL20) and some factors, such as CCL2, were common for both cell types. Vascular endothelial growth factor (VEGF) can also modulate tumour immunity by inducing macrophage and myeloid-derived suppressor cells (MDSCs) recruitment[38] and we previously showed that it is an OSMR target[35]. As seen in Fig. 6d, VEGF levels were increased upon OSM treatment both in CAFs and tumours cells. As some of the OSM-induced chemokines are potent myeloid chemoattractants (i.e. VEGF, CCL2, CXCL12[39,40]), we sought to determine whether myeloid cell populations were altered in tumours after OSMR signalling abrogation. We performed immunostaining of macrophages and neutrophils, assessed by F4/80 and Ly6G positivity respectively[3,41,42], and we observed that these two populations were reduced in MMTV-PyMT: OSMR KO tumours compared to OSMR WT tumours (Fig. 6e). Interestingly, VEGF, CXCL1 and CXCL16 levels were reduced in the serum of tumour bearing MMTV-PyMT: OSMR KO mice compared to control mice (Fig. 6f), all factors being involved in myeloid cell recruitment[38,43,44]. In summary, these results show that macrophages and neutrophils are reduced in OSMR deficient tumours and that chemokines induced by OSM in tumour cells and in stroma may be responsible for myeloid cell recruitment. Our findings are clinically relevant as VEGF, CXCL1 and CXCL16 mRNA expression is associated with decreased recurrence-free survival in breast cancer patients (Fig. 6g), and strongly correlated with OSM and/or OSMR levels (Fig. 6h).

As OSM is mainly expressed by myeloid cells (Figs. 3 and 4), our data point to the existence of a feedback positive loop where OSM signalling in both cancer cells and CAFs induces the

recruitment of more myeloid cells which will in turn secrete more OSM within the tumour. Moreover, conditioned media from cancer cells pre-treated with OSM further increased OSM expression in macrophage-like differentiated HL-60 cells (Fig. 6i). We did not observe this effect with conditioned media from OSM-activated CAFs or with OSM itself. These results suggest that OSMR activation in cancer cells, not only increases the secretion of chemokines involved in myeloid cell recruitment, but also induces OSM expression in these myeloid cells, doubly contributing to the aforementioned feed-forward loop.

**Discussion**

Cytokines are important players in inflammation, a process associated with tumour progression[5]. Even the cancers not directly associated with persistent infections or chronic inflammation, such as breast cancer, exhibit tumour-elicited inflammation, which has important consequences in tumour promotion, progression and metastasis[6,20]. Understanding how inflammatory signals orchestrate pro-malignant effects in the different cell compartments within the tumour microenvironment is key to design new therapeutic strategies to target tumour-promoting inflammation. Our study identifies the pro-inflammatory cytokine OSM as a crucial mediator of the crosstalk between different cell types within the tumour by activating an intriguing pro-tumoural "*ménage-à-trois*" between myeloid cells, CAFs and cancer cells (Fig. 7). By analysing multiple datasets of clinical samples and a wide array of animal and cellular models, we demonstrated that myeloid derived OSM promotes tumour progression by activating the stroma. OSM activates CAFs by increasing their contractility and proliferation. In addition, OSM activates a pro-inflammatory signature in CAFs and cancer cells which, in turn, recruit more myeloid OSM-secreting cells and induce OSM expression by macrophages, establishing a feed forward positive loop (Fig. 7).

Our single cell RNA-seq and FACS sorting analyses revealed that OSM and OSMR have a unique expression pattern in breast tumours, compared to other members of the IL6 cytokine family (Fig. 2 and Extended Data Fig.2). While the ligand OSM was only expressed by the myeloid cell populations, we found that the receptor OSMR was mainly expressed by fibroblasts, cancer and endothelial cells. Our data resonate well with other reports describing OSM secretion by leukocytes (myeloid but also T cells) and OSMR expression in stromal cells (i.e. fibroblasts, endothelial cells, muscle cells, adipocytes and osteoblasts) in different physiopathological contexts[26]. In our hands, the T cell compartment exhibits little or no OSM expression and its production is restricted to myeloid cells. Whether there is one myeloid cell population mainly responsible for OSM production in breast cancer, or whether OSM is secreted by different immune cell types (including neutrophils, TAMs and MDSCs) remains to be determined. Of interest, our analysis of clinical breast cancer samples revealed a significant positive correlation between OSM expression and presence of monocytes, macrophages, and neutrophils, being the latter the cell population that showed the strongest association with OSM (Extended Data Fig. 4a). Importantly, a recent report identified OSM as one of the key signalling mediators of neutrophil-cancer cell interactions in pro-metastatic clusters of neutrophils and circulating tumour cells (CTCs)[45].

The cell population showing the most significant association with OSMR expression in human breast cancer samples is the cancer-associated fibroblasts compartment, suggesting an important role for this cell type in transducing OSM signalling in the tumour. In fact, our co-injections of human immortalized CAFs with breast cancer cells demonstrated that activation of OSMR by OSM in fibroblasts leads to a more aggressive cancer phenotype. While the pro-tumoural effect of OSMR activation in cancer cells has been extensively described[11,12,46], little is known about the effects of OSM in the tumour stroma and our results shed light on the effects of OSM signalling in CAFs. It has been previously reported that OSM stimulates actomyosin contractility and matrix remodelling by oral SCC derived CAFs[47]. In addition to an effect in

contractility, we observed an increase in proliferation and a pro-inflammatory phenotype of OSM activated CAFs. OSM also induces in CAFs the expression of *bona fide* activation markers such as FAP and periostin. Importantly, a signature comprising the top 4 OSM target genes in CAFs (SERPINB4, THBS1, RARRES1 and TNC) is associated with decreased recurrence-free survival (Fig.1, Extended Fig.1 and 4e). Tenascin C (TNC) and Thrombospondin 1 (THBS1) are extracellular matrix proteins involved in cell adhesion, and abundant in breast cancer stroma[48]. RARRES1 (also known as TIG1) has been involved in breast cancer progression[49] and SERPINB4 is up-regulated in many cancer types[50].

In addition to the aforementioned effects, OSM induces in CAFs, but also in cancer cells, the secretion of important myeloid chemoattractants. Some of them are fibroblast-specific (i.e. CXCL10, CXCL12and CXCL16), others are cancer cell-specific (e.g. CXCL7) and several are induced by both cell types (e.g. VEGF, CCL2 and CXCL1), supporting activation of cell-specific transcriptional programmes by OSM[51]. To our knowledge, this is the first report describing that OSM induces the activation of a pro-inflammatory transcriptional programme in CAFs. In line with our results, a similar pro-inflammatory programme was described to be activated by OSM in intestinal stromal cells in inflammatory bowel disease[52]. Regarding OSM effects in cancer cells, we and others have previously described OSM-mediated induction of VEGF and CXCL1[35,53]. However, we have identified herein new OSM targets in cancer cells, as the neutrophil chemoattractant CXCL7, previously described as a prognostic factor in clear cell renal cell carcinoma[54]. Of interest, VEGF, CXCL1 and CXCL16 were found to be downregulated in the serum of MMTV-PyMT OSMR deficient mice, indicating that OSM signalling also regulates their secretion *in vivo.* As mentioned in the results section, these chemokines are important myeloid chemoattractants[38,43,44]. The list of OSM-induced chemokines includes CCR2 and CXCR2 ligands (i.e. CXCL1, CXCL8 and CCL2). Of interest, inhibition of recruitment of MDSCs by blocking CCR2 and CXCR2 activation disrupts the formation of pre-metastatic niches and inhibits metastasis[55].

Importantly, our results reveal that OSM signalling promotes the recruitment of Ly6G+ and F4/80+ myeloid cells to the tumour through OSM-induced secretion of chemokines by both CAFs and cancer cells. These recruited myeloid cells will then increase the secretion of OSM within the tumour, inducing a feed-forward loop. Decreased numbers of Ly6G+ neutrophils and F4/80+ macrophages may explain, at least in part, the strong antitumoural and anti-metastatic effect of OSMR depletion in the PyMT cancer model, as blocking neutrophil recruitment to the pre-metastatic niche with anti-Ly6G antibodies inhibits metastasis[56] and impairing recruitment of tumour-associated macrophages (TAMs) reduces tumour incidence and metastasis[57–59] in MMTV-PyMT mice. Ly6G is also considered a marker of granulocytic MDSCs[3]. Of interest, these cells are involved in the promotion of metastasis in the PyMT model[60].

In addition, we also observed that cancer cells, but not CAFs, contribute further to the OSM-induced feed-forward loop by promoting OSM secretion in macrophages. Tumour-cell secreted factors induce secretion of STAT3 activators in macrophages[61]. It has also been described that OSM induces macrophage migration and polarization towards a M2-like pro-tumoural phenotype[16]. Our results show that immune cells and HL-60 cells differentiated to macrophages with TPA express very little OSMR, bringing up the possibility that OSM affects macrophage polarization and migration through other mechanisms and not by direct OSMR activation.

In summary, our results prove that OSM orchestrates an intriguing pro-tumoural crosstalk between myeloid cells, CAFs and cancer cells that has important consequences in tumour progression. Constitutive genetic depletion of OSMR in the MMTV-PyMT genetic mouse model delays tumour onset, reduces tumour growth and lung metastasis. In addition, injection of murine cancer cells in OSMR deficient mice reduced tumour burden and delayed tumour onset compared to WT mice, supporting that OSM signalling is important in both the stroma and

cancer cell compartment. Breast cancer metastasis is the main cause of death in patients and finding new therapeutic targets for the advanced disease is an unmet need with high clinical impact. Importantly, we found that OSMR depletion in the MMTV-PyMT breast cancer model has a profound effect in reducing metastasis, compared to its effect in tumour onset and tumour growth (Fig. 2). In view of these results, the role of OSM:OSMR signalling in the pre-metastatic niche requires further investigation.

Analysis of human breast cancer samples revealed that our results are clinically relevant, showing that OSM and its receptor OSMR are upregulated in breast cancer stroma, and OSM expression and its transcriptional signature are associated with decreased survival. OSM:OSMR interactions could be blocked by antibody based inhibition, a strategy that has had a major impact on cancer[62], which makes them a promising candidate for therapeutic targeting. Interestingly, anti-OSM humanized antibodies have proven to be safe and well tolerated[19] and are now in Phase 2 clinical trials for the treatment of inflammatory diseases, such as systemic sclerosis and Crohn's disease. Together, our findings further strengthen the case for the pre-clinical investigation of OSM:OSMR blocking antibodies as a targeted anti-cancer therapy.

## Methods

**Tissue Microarrays.** Formalin-fixed and paraffin-embedded blocks of 141 tumour tissues from cases surgically resected at the University Hospital Basel between 1991 and 2013, and included in tissue microarrays (TMAs), were used for analysis of OSM protein expression in human samples. All patients have given informed consent for their archival tissue to be used for scientific research, and the TMA construction was authorized by the Hospital Ethic Committee. TMAs were generated by punching 1 mm spot of each sample. Complete histopathological information, date and cause of death, as well as date of local and/or distant relapse were available for all the patients. Tissue sections were subjected to a heat-induced antigen

retrieval step prior to exposure to primary OSM antibody (1:50, HPA029814, Sigma-Aldrich). Immunodetection was performed using the Roche Ventana BenchMark ULTRA IHC/ISH staining system, with DAB as the chromogen. Cases were reviewed by two independent pathologists and OSM staining was evaluated by the semiquantitative method of H-score (or "histo" score), used to assess the extent of immunoreactivity in tumour samples[63]. Inflammation was assessed by a pathologist as high or low tumour infiltration of immune cells according to their morphology.

**Gene expression analysis of clinical datasets and bioinformatics analysis.** Disease-free survival (DFS) of patients based on OSM mRNA expression was calculated using data from the publicly available METABRIC[21] and Wang datasets[22] with the CANCERTOOL interface[64]. Kaplan-Meier curves showing overall (OS) or relapse-free survival (RFS) of patients from various cancer types according to the expression of different genes by RNA-seq-analysis were obtained from Kaplan-Meier Plotter website[23]. Best threshold cutoffs were selected automatically by the program. RNA-seq data from 64 cell lines was retrieved from the Human Protein Atlas[28] (https://www.proteinatlas.org/). RNA consensus normalized expression values (NX) were plotted for OSM and OSMR transcripts using GraphPad software. Correlations between OSMR and OSM mRNA expression and enrichment of different cell types were analysed by using xCell[30] (https://xcell.ucsf.edu/) on 1809 breast cancer samples from Kaplan-Meier Plotter website[33] and TIMER2.0 (http://timer.cistrome.org/) which incorporates 1100 breast cancer samples from TCGA[31]. TIMER2.0 was also used to analyse gene expression correlations, after purity adjustment. All correlations were calculated with the Spearman's rank correlation coefficient. Gene expression analyses of human tumour stroma and epithelia were retrieved from NCBI Gene Expression Omnibus (GEO): Finak (GSE9014, Breast)[65], Casey (GSE10797, Breast)[66], Yeung (GSE40595, Ovary)[67], Nishida (GSE35602, Colon)[68], and Calon (GSE39396, Colon)[69]. For Affimetrix-based arrays, probe-to-gene mapping was performed using Jetset, while for the rest, highest variance probes were selected. Unless otherwise stated, expression

values for each gene were z-score normalized. GO analysis was performed using Panther[70] (http://pantherdb.org/).

**Single-cell RNA sequencing (scRNA-seq).** Drop-seq dataset[71] raw data for MMTV-PyMT (WT) tumours were obtained from Valdes-Mora *et al. (2020)*[72]. This subset was subsequently analysed using Seurat[73] (v Seurat 3.2). Briefly, a total of 9,636 sequenced cells from 8 MMTV-PyMT tumours pass the QC filter, with <5% mitochondrial to nuclear gene content[71], and <8,000 molecules/cell as they potentially represented cell doublets. Downstream analysis was performed according to Butler *et al. (2018)*[73], using 30 principal components to build a Shared Nearest Neighbour (SNN) graph calculating k-nearest neighbour (Jaccard Index) for each cell, subsequent cluster calling and UMAP dimensional reduction projection[74].

**Cell culture.** Human breast cancer-associated (CAF-173, CAF-200, CAF-220 and CAF-318) and normal fibroblasts (RMF-31 and RMF-39) were derived from human breast tumours and reduction mammoplasty surgeries respectively, immortalized, tagged with GFP and cultured in collagen pre-coated flasks[34]. The aforementioned human mammary fibroblasts, TS1 cells derived from primary tumours of the MMTV-PyMT mice model[27,75], LM2 breast cancer cells (kindly donated by Dr. Roger Gomis) and HS27 skin fibroblasts (kindly donated by Dr. Ander Izeta) were cultured in DMEM medium supplemented with 10% fetal bovine serum (FBS), 1% glutamine, and 1% penicillin and streptomycin. HL-60 promyeloblast cell line, the human embryonic kidney cell line HEK293T and human breast cancer cell lines (MDA-MB-231, BT-549, HCC38, MDA-MB-157, SUM149PT, HCC1806, HCC70, MDA-MB-468, HCC1569, HCC1954, SK-BR-3, MDA-MB-453, CAMA-1, ZR-75-1, T47D, MCF-7, BT-474) were purchased from American Type Culture Collection (ATCC) and cultured following ATCC instructions. All cell lines were authenticated by short tandem repeat profiling (Genomics Core Facility at “Alberto Sols” Biomedical Research Institute) and routinely tested for mycoplasma contamination. HL-60

differentiation to macrophages was achieved by adding 1nM of phorbol 12-myristate 13-acetate (TPA) for 24 hours.

**Generation of OSM overexpressing and OSMR knock-down cells.** MDA-MB-231 cells were stably transfected with 2 µg of pUNO1-hOSM expression construct (InvivoGen), using TurboFect$^{TM}$ followed by Blasticidin (Sigma-Aldrich) selection at 10 µg/ml. Control transfections were performed simultaneously using 2 µg of empty vector. For OSMR knockdown in CAF-173 cells, pLKO-puro-shOSMR lentiviral vectors were purchased from Sigma-Aldrich (NM_003999.1-1342S21C1). Lentiviral infections were performed as previously described[76].

**Collagen cell contraction assays.** To assess the collagen remodelling capacity[77], fibroblasts were treated for 4 days with recombinant human OSM (R&D Systems) at 10 ng/µl or vehicle (PBS) before being embedded in collagen (2mg/ml, Corning). After polymerization, collagen gels were detached, and they were treated with OSM (10ng/ml) or vehicle. Pictures were taken 48 hours later, and the area of collagen disks was analysed using Fiji-Image J software.

**3D fibroblast cell cultures**. Fibroblast spheres were formed seeding 8000 cells/well in 96-well ultra-low attachment Corning plates (Costar). Cells were treated with 30 ng/µl OSM or PBS for 3 (for transcriptomic microarray analysis) or 4 days (for RT-qPCR, Western Blot analysis and quantification of spheres area). Pictures were taken using EVOS FL Cell Imaging System (ThermoFisher) and area of spheres was analysed using Fiji-Image J software. Spheres were collected for RNA and protein analysis.

**Mouse studies.** All procedures involving animals were performed with the approval of the Biodonostia Animal Experimentation Committee and Gipuzkoa Regional Government, according to European official regulations. Generation of the congenic strain MMTV-PyMT:OSMR-/- was accomplished by mating MMTV-PyMT mice (FVB/N-Tg(MMTV-PyVT)634Mul/J, The Jackson Laboratory) with OSMR$^{-/-}$ (OSMR KO, B6.129S-Osmr<tm1Mtan>, Riken BRC)[78,79]. To transfer the OSMR KO line (with a C57BL/6J background) to the genetic

background of the tumour-prone animals (FVB/NJ), the OSMR KO mice were previously backcrossed with FVB/NJ mice for 9 generations. Animals used for experiments were female littermates. Tumours were measured once a week using an external calliper and volume was calculated as $(4\pi/3) \times (\text{width}/2)^2 \times (\text{length}/2)$. Animals were culled at 14 weeks, once tumours in the control group reached the maximum allowed size. Tumour burden was calculated by adding the volume or the weight of all the tumours from the same animal. For whole-mount analysis of preneoplastic lesions, abdominal mammary glands from 9 week-old MMTV-PyMT:OSMR-/- and control female mice were spread out on a glass slide, fixed overnight in Carnoy's solution, stained with Carmine Alum and cleared in ethanol and xylene. Pictures were taken with a Nikon D5000 at 60mm focal length. For the generation of syngeneic orthotopic tumours, 300.000 viable TS1 cells in growth factor reduced (GFR) matrigel (1:1 ratio, Corning), were injected into the fourth right mammary fat pad of anesthetized (with 4% isoflurane) 6-8 week-old OSMR KO or control mice. For the orthotopic co-injections of MDA-MB-231 breast cancer cells and CAF-173 CAFs, cells were injected into the fourth right mammary fat pad of anesthetized (with 4% isoflurane) 6 week-old Athymic Nude-Foxn1nu (Charles River). In OSM activation experiments, CAF-173 were treated with 10 ng/µl OSM for 4 days, prior to co-injection with MDA-MB-231 (500.000 cells each cell line) in GFR matrigel (Corning, 1:1 ratio). For OSMR knockdown experiments, 100.000 MDA-MB-231 hOSM cells and 500.000 CAF-173 shOSMR CAFs were co-injected in GFR matrigel. Animals were monitored 3 times a week and tumour growth measured using an external calliper. Animals were culled once tumours reached the maximum allowed size. In all mouse experiments, after animal culling lungs were visually inspected for macroscopic metastases, and mammary glands and lungs were fixed in neutral buffered formalin solution (Sigma-Aldrich). Microscopic metastases were determined by H&E staining of formalin-fixed paraffin-embedded sections. Tumours were divided in portions for 1) preparation of tissue sections for H&E and IHC staining (fixed in formalin) and 2) protein and RNA extraction (snap frozen).

**Flow cytometry sorting.** TS1 cells were injected orthotopically in FVB mice as described above, and 15 days after injection, freshly obtained TS1 tumours were dissociated into single cell suspension and stained with the antibodies described in Supplementary Table 1. Flow sorting was performed with a BD FACSAria II cell sorter. Gating strategy for experiments is shown in Extended Data Fig 3a. A pool of 4 tumours from 4 animals were used for each sorting experiment. MMTV-PyMT tumours were sorted by Ferrari *et al*. (2019)[80] and RNA from FACS sorted tumours was kindly provided by Fernando Calvo. Briefly, tumour populations were separated into fibroblasts (PDGFRA+), cancer (EPCAM+), immune (CD45+), endothelial cells (CD31+), and the remaining population that was negative for all markers.

**Western blotting.** Cells and tumours were lysed in RIPA buffer supplemented with protease and phosphatase inhibitors (cOmplete™ ULTRA Tablets, Mini, EASYpack Protease Inhibitor Cocktail, and PhosSTOP, both from Roche). Total lysates were resolved by SDS/PAGE and transferred to nitrocellulose membranes. After blocking with 5% (wt/vol) nonfat dry milk in TBS-Tween, membranes were incubated with the corresponding antibodies (Supplementary Table 1) overnight at 4 °C. Secondary antibodies were chosen according to the species of origin of the primary antibodies and detected by an enhanced chemiluminescence system (Bio-Rad). Densitometric analysis of the relative expression of the protein of interest versus the corresponding control (β-actin or total STAT3) was performed with Fiji-Image J software. Uncropped images used to display blots in the main figures can be found in Supplementary Figure 1.

**DNA/RNA extraction, RT-qPCR and transcriptomic analysis.** Lung genomic DNA was extracted from frozen lungs using the QIAmp DNA mini kit (Qiagen) for qPCR analysis. RNA was obtained from snap frozen animal tissue or cell pellets and extracted using TRIzol reagent (Invitrogen) or Recover all Total Nucleic Acid Isolation kit (Invitrogen), for qRT-PCR and microarray analysis, respectively. cDNA was obtained with the Maxima first strand cDNA synthesis kit (Thermo

Scientific) with DNAse treatment incorporated. qPCR was performed using Power SYBR Green PCR master mix (Applied Biosystems), oligonucleotides sequences are described in Supplementary Table 2 and were purchased from Condalab. Expression levels of genes were determined using the ΔΔCt method[81] and normalized against 3 housekeeping genes optimized for each reaction[82]. Human Alu sequences[36] were normalized against 18s housekeeping gene capable of recognizing both human and mouse DNA. Microarray analysis was performed using Human Clariom S assay (ThermoFisher). RNA quality was evaluated using the 2100 Bioanalyzer (Agilent) and microarray chips were processed on the Affymetrix GeneChip Fluidics Station 450 and Scanner 3000 7G (Affymetrix) according to standard protocols. Data were analysed using the Transcriptome Analysis Console 4.0 (TAC). Genes with FDR<0.1 and fold change >2 were considered significantly modulated. GSEA was performed as previously described[37]. FDR < 0.25 or 0.05 was regarded as statistically significant, depending on the type of permutations performed. We compiled the GSEA signatures used in Fig. 5 and 6 and Extended Data Fig. 5 from the Molecular Signatures Database (MsigDB) by the Broad Institute or they were manually curated from the literature. The gene list for each signature is publicly available at http://software.broadinstitute.org/gsea/msigdb/search.jsp, Pein *et al*. (2020)[83] or in Supplementary Tables 3 and 4.

**Histopathology and Immunohistochemistry (IHC) analysis.** Histological analysis of tumours and lung metastasis was performed in formalin-fixed paraffin-embedded haematoxylin-eosin stained sections. Immunohistochemical staining was performed in formalin-fixed paraffin-embedded sections using the streptavidin–biotin–peroxidase complex method. Antigen retrieval was performed using boiling 10 mM citrate buffer, pH 6.0, for 15 min. Endogenous peroxidase activity was inactivated by incubation with 3% hydrogen peroxide in methanol (15 min, at room temperature). Tissue sections were incubated in a humidified chamber (overnight, 4 ºC) using the antibodies described in Supplementary Table 1 diluted in Tris-buffered saline (TBS). For negative controls, primary antibodies were replaced by non-immune

serum. After three rinses in TBS (5 min each), samples were incubated with the corresponding secondary antibody (Supplementary Table 1). After 30 min incubation, tissue sections were washed in TBS (5 min, 3 times) and immediately incubated for 30 min with streptavidin–peroxidase complex diluted 1:400 in TBS (Invitrogen). The chromogen was 3-30-diaminobenzidine (Vector Laboratories). Nuclei were counterstained with Harris haematoxylin for 1 min. Pictures were obtained using the Nikon Eclipse 80i microscope with the Nikon DS-5M camera incorporated. The number of positive cells and total cells per area was counted manually in 5-10 different areas of samples from 5 mice per experimental group, using Fiji-Image J software.

**Cytokine and chemokine analysis.** Cytokine and chemokine levels were analysed in conditioned media from CAF-173 treated with OSM (30 ng/mL) or vehicle for 72 hours, and from MDA-MB-231-hOSM and corresponding control cells (n = 4 independent experiments). A panel of 31 human chemokines was analysed by Human Chemokine Array Kit (Proteome Profiler Array, R&D Systems), and VEGF levels were quantified by Human VEGF Quantikine ELISA Kit (R&D Systems) following the manufacturer's instructions. Mouse VEGF, CXCL1 and CXCL16 levels on plasma from 14-week-old MMTV-PyMT: OSMR KO, HET and WT mice were analysed by mouse Premixed Multi-Analyte Kit (Magnetic Luminex Assay, R&D Systems) following the manufacturer's instructions. Detection was carried out with the MAGPIX® detector and data analysis was performed using the xPOTENT® software, both from R&D Systems.

**Statistical analyses.** Statistical analyses were performed using GraphPad Prism or SPSS software. For Gaussians distributions, the student's t-test (paired or unpaired) was used to compare differences between two groups. Welch's correction was applied when variances were significantly different. One-way ANOVA was used to determine differences between more than two independent groups. For non-Gaussian distributions, Mann–Whitney's test was

performed. Chi-square test was used to determine differences between expected frequencies. For Kaplan-Meier analysis the Log-rank (Mantel-Cox) test was used. P values inferior to 0.05 were considered statistically significant. Unless otherwise stated, results are expressed as mean values +/- standard errors (SEM).

**Data availability.** RNA-seq raw data were obtained from Valdes-Mora *et al.* (2020)[72] https://www.biorxiv.org/content/10.1101/624890v3. The datasets generated during the current study will be available in the GEO repository upon publication. A confidential reviewer link can be facilitated upon request. Source data on uncropped Western blots are provided in Supplementary Figure 1. The gene list for the fibroblast activation markers signature used in Fig. 5 was derived from Sahai *et al*. (2020)[25] and is shown in Supplementary Table 3. The gene list for the CAF-173 OSM signature used in Extended Data Fig. 5 includes the 233 genes differentially upregulated in CAF-173 upon OSM treatment and can be found in Supplementary Table 4. Source data for Figs. 1–6 and Extended Data Figs. 1–6 will be provided upon publication and can be facilitated to reviewers upon request. All other data files supporting the findings of this study are available from the corresponding author upon reasonable request.

## Acknowledgements

We are grateful to the members of our laboratories for critical discussion of this work and to the Genomics and Histology Platforms and Animal Facility of the Biodonostia Health Research Institute and Onkologikoa Foundation for technical assistance and advice. We thank Dr Eva González-Suarez (CNIO, Madrid, Spain) and Dr William Muller (McGill University, Montreal, Canada) for providing the MMTV-PyMT mice, and Dr Ander Izeta (IIS Biodonostia, San Sebastian, Spain) and Dr Roger Gomis (IRB, Barcelona, Spain) for providing the HS27 fibroblasts and LM2 cells respectively. This work was funded by Spanish Ministry of Economy and Competitiveness (PI15/00623, PI18/00458 and CP18/00076) and European Regional

Development (FEDER) funds, Basque Department of Health (2017111011), Fundación SEOM (Beca SEOM-Font Vella) and Ikerbasque Basque Research Foundation. A.Araujo and A.Abaurrea are funded by Basque Government Doctoral Training Grants and Fundación Gangoiti. JILV is funded by a PFIS Doctoral Training Grant from the Spanish Ministry of Economy and Competitiveness (FI19/00193).

**Author Contributions**

A.Araujo, A.Abaurrea, PA and IOQ performed all the cellular and molecular experiments. A.Araujo, A.Abaurrea and MMC performed the animal experiments. JMF performed immunohistochemistry and analysed mouse histopathology. JILV analysed mouse immunostaining. FVM and DGO obtained and analysed the scRNAseq data. A.Araujo, LJ, NF and FC performed FACS-Sorting. AT and SEP collected and analysed patient data and generated the TMAs. RR and MMC analysed the TMA staining. A.Abaurrea, PA, NMM, FC and AC performed bioinformatic analysis. PFN and PB generated the fibroblast cell lines. NC, IAL and AU contributed with experimental design. CI and CHL contributed with experimental design and helped with supervision of the project. A.Araujo and MMC designed and supervised the study, analysed the data and wrote the manuscript. All authors gave final approval to the submitted and published versions of the manuscript.

**Competing Interests statement**

The authors declare no conflict of interest.

**References:**

1. Hanahan, D. & Weinberg, R. A. Hallmarks of cancer: the next generation. *Cell* **144**, 646–674 (2011).

2. Greten, F. R. & Grivennikov, S. I. Inflammation and Cancer: Triggers, Mechanisms, and Consequences. *Immunity* **51**, 27–41 (2019).

3. Quail, D. F. & Joyce, J. A. Microenvironmental regulation of tumor progression and metastasis. *Nat. Med.* **19**, 1423–1437 (2013).

4. Kalluri, R. The biology and function of fibroblasts in cancer. *Nat. Rev. Cancer* **16**, 582–598 (2016).

5. Hanahan, D. & Coussens, L. M. Accessories to the Crime: Functions of Cells Recruited to the Tumor Microenvironment. *Cancer Cell* **21**, 309–322 (2012).

6. Taniguchi, K. & Karin, M. IL-6 and related cytokines as the critical lynchpins between inflammation and cancer. *Semin. Immunol.* **26**, 54–74 (2014).

7. Fisher, D. T., Appenheimer, M. M. & Evans, S. S. The two faces of IL-6 in the tumor microenvironment. *Semin. Immunol.* **26**, 38–47 (2014).

8. Zarling, J. M. *et al.* Oncostatin M: a growth regulator produced by differentiated histiocytic lymphoma cells. *Proc. Natl. Acad. Sci. U. S. A.* **83**, 9739–9743 (1986).

9. Guo, L. *et al.* Stat3-coordinated Lin-28-let-7-HMGA2 and miR-200-ZEB1 circuits initiate and maintain oncostatin M-driven epithelial-mesenchymal transition. *Oncogene* **32**, 5272–5282 (2013).

10. Kucia-Tran, J. A. *et al.* Overexpression of the oncostatin-M receptor in cervical squamous cell carcinoma is associated with epithelial-mesenchymal transition and poor overall survival. *Br. J. Cancer* **115**, 212–222 (2016).

11. Caffarel, M. M. & Coleman, N. Oncostatin M receptor is a novel therapeutic target in cervical squamous cell carcinoma. *J. Pathol.* **232**, 386–390 (2014).

12. Jahani-Asl, A. *et al.* Control of glioblastoma tumorigenesis by feed-forward cytokine signaling. *Nat. Neurosci.* **19**, 798–806 (2016).

13. West, N. R., Murphy, L. C. & Watson, P. H. Oncostatin M suppresses oestrogen receptor-α expression and is associated with poor outcome in human breast cancer. *Endocr. Relat. Cancer* **19**, 181–195 (2012).

14. Tawara, K. *et al.* HIGH expression of OSM and IL-6 are associated with decreased breast cancer survival: Synergistic induction of IL-6 secretion by OSM and IL-1β. *Oncotarget* **10**, 2068–2085 (2019).

15. Kan, C. E., Cipriano, R. & Jackson, M. W. c-MYC functions as a molecular switch to alter the response of human mammary epithelial cells to oncostatin M. *Cancer Res.* **71**, 6930–6939 (2011).

16. Tripathi, C. *et al.* Macrophages are recruited to hypoxic tumor areas and acquire a Pro-

Angiogenic M2-Polarized phenotype via hypoxic cancer cell derived cytokines Oncostatin M and Eotaxin. *Oncotarget* **5**, 5350–5368 (2014).

17. Angevin, E. *et al.* A phase I/II, multiple-dose, dose-escalation study of siltuximab, an anti-interleukin-6 monoclonal antibody, in patients with advanced solid tumors. *Clin. Cancer Res.* **20**, 2192–2204 (2014).

18. Kang, S., Tanaka, T., Narazaki, M. & Kishimoto, T. Targeting Interleukin-6 Signaling in Clinic. *Immunity* **50**, 1007–1023 (2019).

19. Reid, J. *et al.* In vivo affinity and target engagement in skin and blood in a first-time-in-human study of an anti-oncostatin M monoclonal antibody. *Br. J. Clin. Pharmacol.* **84**, 2280—2291 (2018).

20. Tower, H., Ruppert, M. & Britt, K. The Immune Microenvironment of Breast Cancer Progression. *Cancers (Basel).* **11**, (2019).

21. Curtis, C. *et al.* The genomic and transcriptomic architecture of 2,000 breast tumours reveals novel subgroups. *Nature* **486**, 346–352 (2012).

22. Wang, Y. *et al.* Gene-expression profiles to predict distant metastasis of lymph-node-negative primary breast cancer. *Lancet* **365**, 671–679 (2005).

23. Nagy, Á., Lánczky, A., Menyhárt, O. & Gyorffy, B. Validation of miRNA prognostic power in hepatocellular carcinoma using expression data of independent datasets. *Sci. Rep.* **8**, 1–9 (2018).

24. Lin, E. Y. *et al.* Progression to Malignancy in the Polyoma Middle T Oncoprotein Mouse Breast Cancer Model Provides a Reliable Model for Human Diseases. *Am. J. Pathol.* **163**, 2113–2126 (2003).

25. Sahai, E. *et al.* A framework for advancing our understanding of cancer-associated fibroblasts. *Nat. Rev. Cancer* **20**, 174–186 (2020).

26. West, N. R., Owens, B. M. J. & Hegazy, A. N. The oncostatin M-stromal cell axis in health and disease. *Scand. J. Immunol.* **88**, (2018).

27. Shree, T. *et al.* Macrophages and cathepsin proteases blunt chemotherapeutic response in breast cancer. *Genes Dev.* **25**, 2465–2479 (2011).

28. Uhlen, M. *et al.* A pathology atlas of the human cancer transcriptome. *Science* **357**, (2017).

29. Birnie, G. D. The HL60 cell line: A model system for studying human myeloid cell differentiation. *Br. J. Cancer* **58**, 41–45 (1988).

30. Aran, D., Hu, Z. & Butte, A. J. xCell: digitally portraying the tissue cellular heterogeneity landscape. *Genome Biol.* **18**, 220 (2017).

31. Li, T. *et al.* TIMER: A Web Server for Comprehensive Analysis of Tumor-Infiltrating Immune Cells. *Cancer Res.* **77**, e108–e110 (2017).

32. Koboldt, D. C. *et al.* Comprehensive molecular portraits of human breast tumours.

*Nature* **490**, 61–70 (2012).

33. Győrffy, B. *et al.* An online survival analysis tool to rapidly assess the effect of 22,277 genes on breast cancer prognosis using microarray data of 1,809 patients. *Breast Cancer Res. Treat.* **123**, 725–731 (2010).

34. Fernández-Nogueira, P. *et al.* Tumor-Associated Fibroblasts Promote HER2-Targeted Therapy Resistance through FGFR2 Activation. *Clin. Cancer Res.* **26**, 1432–1448 (2020).

35. Kucia-Tran, J. A. *et al.* Anti-oncostatin M antibody inhibits the pro-malignant effects of oncostatin M receptor overexpression in squamous cell carcinoma. *J. Pathol.* **244**, 283–295 (2018).

36. Zijlstra, A. *et al.* A quantitative analysis of rate-limiting steps in the metastatic cascade using human-specific real-time polymerase chain reaction. *Cancer Res.* **62**, 7083–7092 (2002).

37. Subramanian, A. *et al.* Gene set enrichment analysis: A knowledge-based approach for interpreting genome-wide expression profiles. *Proc. Natl. Acad. Sci.* **102**, 15545 LP – 15550 (2005).

38. Yang, J., Yan, J. & Liu, B. Targeting VEGF/VEGFR to modulate antitumor immunity. *Front. Immunol.* **9**, 1–9 (2018).

39. Jahchan, N. S. *et al.* Tuning the Tumor Myeloid Microenvironment to Fight Cancer. *Front. Immunol.* **10**, 1611 (2019).

40. Engblom, C., Pfirschke, C. & Pittet, M. J. The role of myeloid cells in cancer therapies. *Nat. Rev. Cancer* **16**, 447–462 (2016).

41. Coffelt, S. B., Wellenstein, M. D. & De Visser, K. E. Neutrophils in cancer: Neutral no more. *Nat. Rev. Cancer* **16**, 431–446 (2016).

42. Daley, J. M., Thomay, A. A., Connolly, M. D., Reichner, J. S. & Albina, J. E. Use of Ly6G-specific monoclonal antibody to deplete neutrophils in mice. *J. Leukoc. Biol.* **83**, 64–70 (2008).

43. Allaoui, R. *et al.* Cancer-associated fibroblast-secreted CXCL16 attracts monocytes to promote stroma activation in triple-negative breast cancers. *Nat. Commun.* **7**, (2016).

44. Acharyya, S. *et al.* A CXCL1 paracrine network links cancer chemoresistance and metastasis. *Cell* **150**, 165–178 (2012).

45. Szczerba, B. M. *et al.* Neutrophils escort circulating tumour cells to enable cell cycle progression. *Nature* **566**, 553–557 (2019).

46. Stephens, J. M. & Elks, C. M. Oncostatin M: Potential Implications for Malignancy and Metabolism. *Curr. Pharm. Des.* **23**, 3645–3657 (2017).

47. Sanz-Moreno, V. *et al.* ROCK and JAK1 Signaling Cooperate to Control Actomyosin Contractility in Tumor Cells and Stroma. *Cancer Cell* **20**, 229–245 (2011).

48. Kaushik, S., Pickup, M. W. & Weaver, V. M. From transformation to metastasis:

deconstructing the extracellular matrix in breast cancer. *Cancer Metastasis Rev.* **35**, 655–667 (2016).

49. Wang, X. *et al.* TIG1 promotes the development and progression of inflammatory breast cancer through activation of Axl kinase. *Cancer Res.* **73**, 6516–6525 (2013).

50. Sun, Y., Sheshadri, N. & Zong, W.-X. SERPINB3 and B4: From biochemistry to biology. *Semin. Cell Dev. Biol.* **62**, 170–177 (2017).

51. Richards, C. D. The Enigmatic Cytokine Oncostatin M and Roles in Disease. *ISRN Inflamm.* **2013**, 1–23 (2013).

52. West, N. R. *et al.* Oncostatin M drives intestinal inflammation and predicts response to tumor necrosis factor–neutralizing therapy in patients with inflammatory bowel disease. *Nat. Med.* **23**, 579–589 (2017).

53. Bierie, B. *et al.* Abrogation of TGF-β signaling enhances chemokine production and correlates with prognosis in human breast cancer. *J. Clin. Invest.* **119**, 1571–1582 (2009).

54. Grepin, R. *et al.* The CXCL7/CXCR1/2 axis is a key driver in the growth of clear cell renal cell carcinoma. *Cancer Res.* **74**, 873–883 (2014).

55. Lu, Z. *et al.* Epigenetic therapy inhibits metastases by disrupting premetastatic niches. *Nature* **579**, 284–290 (2020).

56. Swierczak, A., Mouchemore, K. A., Hamilton, J. A. & Anderson, R. L. Neutrophils: important contributors to tumor progression and metastasis. *Cancer Metastasis Rev.* **34**, 735–751 (2015).

57. Lin, E. Y., Nguyen, A. V., Russell, R. G. & Pollard, J. W. Colony-stimulating factor 1 promotes progression of mammary tumors to malignancy. *J. Exp. Med.* **193**, 727–739 (2001).

58. Boyle, S. T., Faulkner, J. W., McColl, S. R. & Kochetkova, M. The chemokine receptor CCR6 facilitates the onset of mammary neoplasia in the MMTV-PyMT mouse model via recruitment of tumor-promoting macrophages. *Mol. Cancer* **14**, 1–14 (2015).

59. Strachan, D. C. *et al.* CSF1R inhibition delays cervical and mammary tumor growth in murine models by attenuating the turnover of tumor-associated macrophages and enhancing infiltration by CD8+ T cells. *Oncoimmunology* **2**, 1–12 (2013).

60. Gallego-Ortega, D. *et al.* ELF5 Drives Lung Metastasis in Luminal Breast Cancer through Recruitment of Gr1+ CD11b+ Myeloid-Derived Suppressor Cells. *PLoS Biol.* **13**, (2015).

61. Vlaicu, P. *et al.* Monocytes/macrophages support mammary tumor invasivity by co-secreting lineage-specific EGFR ligands and a STAT3 activator. *BMC Cancer* **13**, (2013).

62. Weiner, G. J. Building better monoclonal antibody-based therapeutics. *Nat. Rev. Cancer* **15**, 361–370 (2015).

63. McCarty, K. S. *et al.* Use of a monoclonal anti-estrogen receptor antibody in the immunohistochemical evaluation of human tumors. *Cancer Res.* **46**, 4244–4249 (1986).

64. Cortazar, A. R. *et al.* Cancertool: A visualization and representation interface to exploit cancer datasets. *Cancer Res.* **78**, 6320–6328 (2018).

65. Finak, G. *et al.* Stromal gene expression predicts clinical outcome in breast cancer. *Nat. Med.* **14**, 518–527 (2008).

66. Casey, T. *et al.* Molecular signatures suggest a major role for stromal cells in development of invasive breast cancer. *Breast Cancer Res. Treat.* **114**, 47—62 (2009).

67. Yeung, T.-L. *et al.* TGF-β modulates ovarian cancer invasion by upregulating CAF-derived versican in the tumor microenvironment. *Cancer Res.* **73**, 5016–5028 (2013).

68. Nishida, N. *et al.* Microarray analysis of colorectal cancer stromal tissue reveals upregulation of two oncogenic miRNA clusters. *Clin. Cancer Res.* **18**, 3054–3070 (2012).

69. Calon, A. *et al.* Dependency of colorectal cancer on a TGF-β-driven program in stromal cells for metastasis initiation. *Cancer Cell* **22**, 571–584 (2012).

70. Mi, H., Muruganujan, A., Ebert, D., Huang, X. & Thomas, P. D. PANTHER version 14: more genomes, a new PANTHER GO-slim and improvements in enrichment analysis tools. *Nucleic Acids Res.* **47**, D419–D426 (2019).

71. Macosko, E. Z. *et al.* Highly Parallel Genome-wide Expression Profiling of Individual Cells Using Nanoliter Droplets. *Cell* **161**, 1202–1214 (2015).

72. Valdes-Mora, F. *et al.* Single cell transcriptomics reveals involution mimicry during the specification of the basal breast cancer subtype. *bioRxiv* 624890 (2020) doi:10.1101/624890.

73. Butler, A., Hoffman, P., Smibert, P., Papalexi, E. & Satija, R. Integrating single-cell transcriptomic data across different conditions, technologies, and species. *Nat. Biotechnol.* **36**, 411–420 (2018).

74. McInnes, L., Healy, J. & Melville, J. UMAP: Uniform Manifold Approximation and Projection for Dimension Reduction. *arXiv*:1802.03426 (2018).

75. Guy, C. T., Cardiff, R. D. & Muller, W. J. Induction of mammary tumors by expression of polyomavirus middle T oncogene: a transgenic mouse model for metastatic disease. *Mol. Cell. Biol.* **12**, 954–961 (1992).

76. Etxaniz, U. *et al.* Neural-competent cells of adult human dermis belong to the Schwann lineage. *Stem cell reports* **3**, 774–788 (2014).

77. Ngo, P., Ramalingam, P., Phillips, J. A. & Furuta, G. T. Collagen gel contraction assay. *Methods Mol. Biol.* **341**, 103–109 (2006).

78. Nakamura, K., Nonaka, H., Saito, H., Tanaka, M. & Miyajima, A. Hepatocyte proliferation and tissue remodeling is impaired after liver injury in oncostatin M receptor knockout mice. *Hepatology* **39**, 635–644 (2004).

79. Tanaka, M. *et al.* Targeted disruption of oncostatin M receptor results in altered hematopoiesis. *Blood* **102**, 3154–3162 (2003).

80. Ferrari, N. *et al.* Dickkopf-3 links HSF1 and YAP/TAZ signalling to control aggressive behaviours in cancer-associated fibroblasts. *Nat. Commun.* **10**, (2019).

81. Pfaffl, M. W. A new mathematical model for relative quantification in real-time RT-PCR. *Nucleic Acids Res.* **29**, e45–e45 (2001).

82. Vandesompele, J. *et al.* Accurate normalization of real-time quantitative RT-PCR data by geometric averaging of multiple internal control genes. *Genome Biol.* **3**, (2002).

83. Pein, M. *et al.* Metastasis-initiating cells induce and exploit a fibroblast niche to fuel malignant colonization of the lungs. *Nat. Commun.* **11**, 1494 (2020).

## Figure Legends

### Fig. 1: OSM correlates with worse clinical prognosis in breast cancer.

**a)** Kaplan-Meier curves showing overall survival (OS) for breast cancer patients whose samples, with high vs. low OSM expression, were included in tissue micro-arrays (TMAs). **b)** Representative pictures of OSM staining in samples with high and low inflammation. **c)** Quantification of OSM staining in tumours with low and high degree of inflammation. **d)** Kaplan-Meier curves showing disease-free survival (DFS) for breast cancer patients, with high vs. low OSM expression, included in the METABRIC dataset.

### Fig. 2: OSMR signalling contributes to tumour progression in the MMTV-PyMT mice model.

**a)** Experimental set up of the *in vivo* experiment designed to assess the importance of OSMR signalling in disease progression of the MMTV-PyMT mouse model. **b-d)** Kaplan-Meier curves for tumour-free survival **(b)**, tumour growth **(c)** and final tumour burden **(d)** in MMTV-PyMT:OSMR wild-type (WT), MMTV-PyMT:OSMR heterozygous (HET), and MMTV-PyMT:OSMR KO mice. In **b)** P value was calculated using the Mantel-Cox test; in **c)** P values were determined in each time point using unpaired two-tailed t test; and in **d)** P value was determined using one-way ANOVA test. **e)** Histopathological analysis of tumours at week 14. Graph represents percentage of mice bearing carcinomas, adenomas, hyperplasia and no lesions in mammary glands. P value was determined comparing malignant (Carcinoma) *vs.* non-malignant phenotypes (Adenoma, hyperplasia) and no lesions using Chi-square test. **f)** Western blot (upper panel) and densitometric analysis (lower panel) of fibronectin protein levels in tumours at week 14 from animals of the different genotypes. P values were determined by the one-way ANOVA test. **g)** Percentage of animals with lung metastases at 14 weeks of age. Lung tumour masses were classified as macrometastases when they were visible at dissection and as micrometastases when they were only detectable by hematoxylin and

eosin staining. P value was determined comparing animals with metastasis (macro and micro) vs. non-metastasis using Chi-square test. **h)** Representative pictures of lung metastases at week 14 in OSMR WT, HET and KO animals. ** p < 0,01; *** p < 0,001.

**Fig. 3: OSM:OSMR signalling is paracrine within the tumour and its pattern of expression differs from other cytokines of the IL-6 family.**

**a)** UMAP plot showing cell clusters defined in each of the main cell lineages. Far right column depicts the main cell lineage of origin for each cluster, showing 7 clusters of epithelial origin, 6 immune and 4 stromal. LP: luminal progenitors, ECM: extracellular matrix, B: basal, ML: mature luminal. **b)** Feature UMAP plots showing the expression of the indicated genes in each of the main cell clusters. **c)** Dot plot representing the expression level (red or blue jet) and the number of expressing cells (dot size) of the indicated genes in each cluster. **d)** Schematic representation of FACS sorting experiments for TS1 orthotopic tumours. The two different experiments were performed independently, each one in a pool of 4 tumours from individual animals. **e)** Osm and Osmr mRNA expression levels analysed by RT-qPCR of FACS sorted populations. Graphs represent mean ± SEM of 3 technical replicates. **f)** mRNA expression levels of the indicated IL-6 family members and associated receptors analysed by RT-qPCR in a panel of breast cancer cell lines and immortalized fibroblasts. In the OSMR graph (bottom panel), green and dark dots represent normal mammary fibroblasts and CAFs, respectively. Graphs represent mean ± SEM. n.s. non-significant. RMF: reduction mammoplasty fibroblasts.

**Fig. 4: OSM:OSMR is elevated in human breast cancer stroma and OSMR signalling in the tumour microenvironment contributes to cancer progression.**

**a)** Correlation of OSMR expression with the enrichment of fibroblasts (left panel), and of OSM expression with enrichment of M2 macrophages and common myeloid progenitors in breast tumours (middle and right panels). Spearman correlation coefficients and P values are shown.

Data were downloaded from xCell cell types enrichment analysis web resource**. b,c)** OSM and OSMR mRNA expression in paired cancer epithelial vs. cancer stroma **(b)** and normal stroma vs. cancer stroma breast cancer samples **(c)**. Data were downloaded from GEO DataSets (GSE10797 and GSE9014). In **b** and **c**, P values were calculated using the unpaired two-tailed t test and graphs represent mean ± SEM. **d)** Experimental set up of the *in vivo* experiment designed to assess the importance of OSMR signalling in the tumour microenvironment, in which TS1 cells were orthotopically injected into the mammary fat pad of OSMR wild-type (WT) and knock-out (KO) mice. **e-g)** Kaplan-Meier curves for tumour-free survival**(e)**, tumour growth **(f)** and final tumour volume and weight after dissection **(g)** of orthotopic tumours generated in OSMR wild-type (WT) and knock-out (KO) mice by injection of TS1 cells into the mammary fat pad. Two independent experiments were performed, and the results were combined in **e** and **g**. **e)** P value was calculated using the Mantel-Cox test. **f,g)** P values were calculated using the unpaired two-tailed t test and graphs represent mean ± SEM. **, p < 0,01.

**Fig. 5: OSM activates cancer-associated fibroblasts (CAFs) *in vitro* and *in vivo* promoting tumour progression.**

**a)** Representative pictures of collagen contraction assays (upper panels) and quantification of collagen disk areas (lower panels) of fibroblasts pre-treated in monolayer with PBS or OSM and seeded in collagen. **b)** Representative pictures (upper panels) and area quantification (lower panels) of 3D spheres proliferation assays of fibroblasts treated with PBS or OSM. In **a** and **b**, graphs represent mean ± SEM and 2 independent experiments are plotted. **c)** RT-qPCR analysis of mRNA levels of activation markers in normal (RMF-31) and cancer-associated fibroblasts (CAF-173) cultured in 3D with PBS or OSM. Graphs represent mean ± SEM of 3 independent experiments. **d)** GSEA showing enrichment of the indicated signatures in microarray data of CAF-173 treated with OSM. **e)** Kaplan-Meier curves showing relapse-free survival (RFS) for breast cancer samples according to the high or low expression of top 4 genes induced by OSM

in CAF-173. Data were obtained using KM plotter website. **f)** Experimental set up of the *in vivo* experiment designed to assess the contribution of OSMR activation in fibroblasts to cancer progression. CAF-173 were pre-treated with OSM or vehicle for 4 days prior to injection and were co-injected with MDA-MB-231 (500.000 cells each cell line) in matrigel (1:1 ratio) in the mammary gland fat pad of nude mice. n=6 animals with MDA-MB-231+ CAF-173 PBS cells injected; and n=7 animals with MDA-MB-231+ CAF-173 OSM cells injected. **g,h)** Tumour growth **(g)** and final tumour volume and weight after dissection **(h)** of orthotopic tumours described in **f)**. Graphs represent mean ± SEM. **i)** Percentage of animals with lung micrometastasis assessed using qPCR analysis of genomic human ALU sequences. Graph represents the percentage of animals with detectable qPCR signal and P value was calculated using the Chi-square test. n.s. non-significant. * $p < 0,05$; *** $p < 0,001$. P values were calculated using the unpaired two-tailed t test unless specified.

**Fig. 6: OSM signalling in CAFs and tumour cells induces cytokine secretion and myeloid recruitment.**

**a)** Heatmaps showing normalized mRNA expression of genes induced by OSM and included in the indicated GO pathways. **b)** GSEA showing enrichment of inflammatory hallmark signature in microarray expression data of CAF-173 spheres treated with PBS (Control) or OSM 30ng/ml for 4 days; and MDA-MB-231 Control or hOSM. **c,d)** Chemokine array analysis **(c)** and VEGF levels **(d)** of conditioned media from CAF-173 treated with PBS (Control) or OSM 30ng/ml for 72 hours or from MDA-MB-231-h-OSM and control cells, 72h after seeding. Graphs represent mean ± SEM (n=4 independent experiments, except for MDA-MB-231 in **c**, where n=3 independent experiments). P values were determined using paired two-tailed t tests. **e)** Representative pictures (left panels) and quantification (right panels) of F4/80 (top panels) and LY6G (bottom panels) immunohistochemistry staining in MMTV-PyMT:OSMR wild-type (WT), heterozygous (HET), and KO mice at 14 weeks of age. Quantification was performed by manual

counting of positive cells per area in a total of 8 pictures per tumour and 5 tumours per group. **f)** VEGF, CXCL1 and CXCL16 levels in plasma from MMTV-PyMT: OSMR WT, HET and KO mice at 14 weeks of age (n=5 per group) analysed by Luminex assay. In **e,f)** graphs represent mean ± SEM (n=5). P values between the different groups were determined using unpaired two tailed t tests. **g)** Kaplan-Meier curves showing relapse-free survival (RFS) for breast cancer samples according to the expression of VEGF, CXCL1 and CXCL16. Data were downloaded from KM plotter. **h)** Correlation of OSM (top) and OSMR levels (bottom panel) with VEGF, CXCL1 and CXCL16 expression in breast cancer. Data were downloaded from TIMER web platform, Spearman correlation coefficients and P values are shown. **i)** OSM mRNA levels in HL-60 + TPA (macrophages) treated with conditioned media from MDA-MB-231 and CAF-173 pre-treated with OSM 10 ng/mL for 72h. Graph represents mean ± SEM of 3 independent experiments. P values were calculated using the paired two-tailed t test.

**Fig. 7: Proposed working model for the effects of OSM signalling in breast cancer.**

Myeloid cells express OSM which activates the OSMR pathway in cancer cells and cancer-associated fibroblasts (CAFs). OSM signalling in CAFs induces classical fibroblast activation markers such as FAP and POSTN as well as induction of pro-tumoural factors (IL6 and VEGF). This paracrine signalling induces CAFs pro-malignant phenotype by increasing their contractility and proliferation. At the same time, OSM induces myeloid chemoattractants in CAFs and cancer cells such as VEGF, CXCL1 and CCXL16. This chemokine secretion results in further myeloid tumour infiltration creating a positive feedback loop that ensures constant liberation of OSM and sustained tumour progression. In addition, cancer cells induce OSM-production in myeloid cells.

# Figure 1

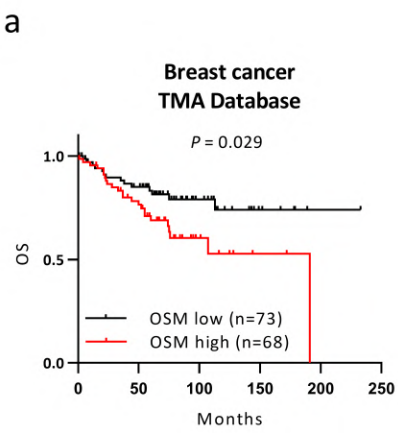
a
Breast cancer
TMA Database
P = 0.029
OS
1.0
0.5
0.0
0
50
100
150
200
250
Months
OSM low (n=73)
OSM high (n=68)

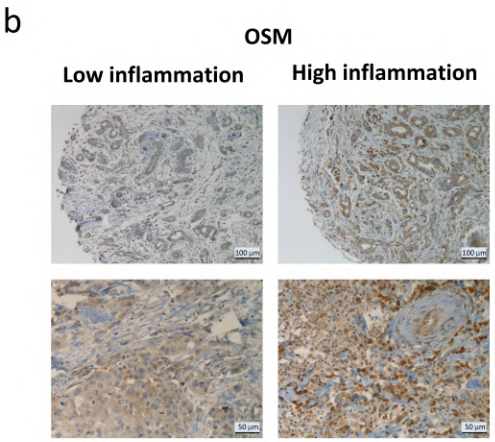
b
OSM
Low inflammation
High inflammation

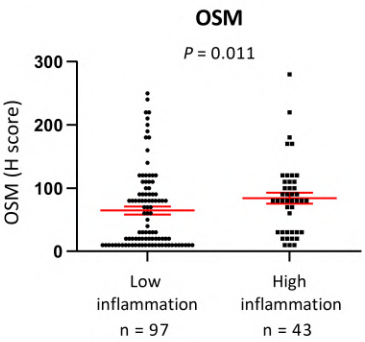
c
OSM
P = 0.011
OSM (H score)
300
200
100
0
Low
inflammation
n = 97
High
inflammation
n = 43

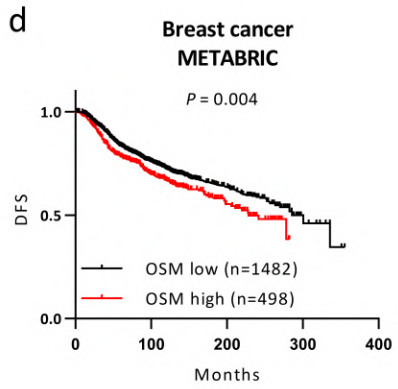
d
Breast cancer
METABRIC
P = 0.004
DFS
1.0
0.5
0.0
0
100
200
300
400
Months
OSM low (n=1482)
OSM high (n=498)

# Figure 2

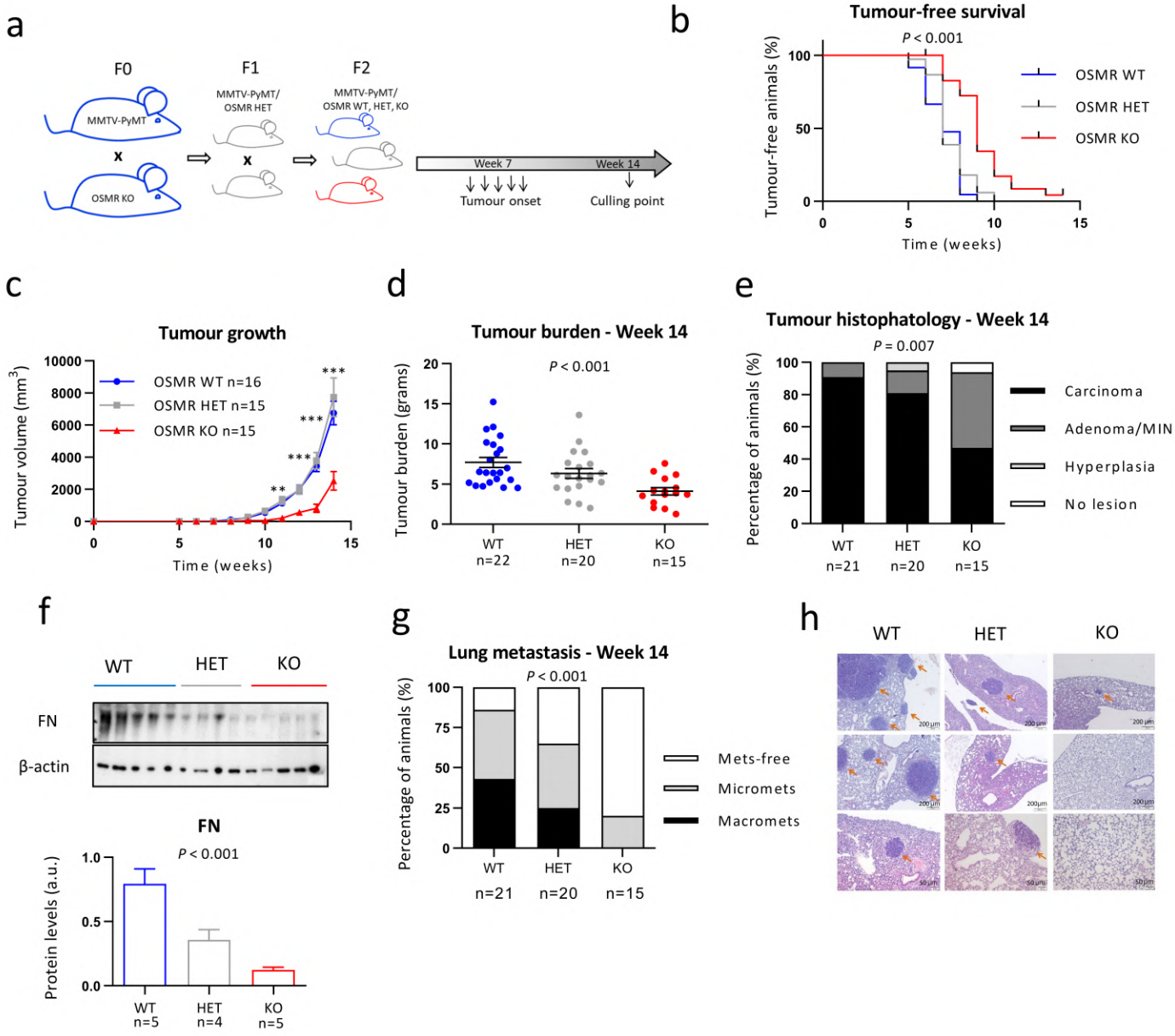
a
F0
F1
F2
MMTV-PyMT
OSMR KO
MMTV-PyMT/
OSMR HET
MMTV-PyMT/
OSMR WT, HET, KO
Week 7
Week 14
Tumour onset
Culling point
b
Tumour-free survival
P < 0.001
Tumour-free animals (%)
Time (weeks)
OSMR WT
OSMR HET
OSMR KO
c
Tumour growth
Tumour volume (mm3)
OSMR WT n=16
OSMR HET n=15
OSMR KO n=15
Time (weeks)
d
Tumour burden - Week 14
P < 0.001
Tumour burden (grams)
WT n=22
HET n=20
KO n=15
e
Tumour histophatology - Week 14
P = 0.007
Percentage of animals (%)
Carcinoma
Adenoma/MIN
Hyperplasia
No lesion
WT n=21
HET n=20
KO n=15
f
WT
HET
KO
FN
β-actin
FN
P < 0.001
Protein levels (a.u.)
WT n=5
HET n=4
KO n=5
g
Lung metastasis - Week 14
P < 0.001
Percentage of animals (%)
Mets-free
Micromets
Macromets
WT n=21
HET n=20
KO n=15
h
WT
HET
KO

# Figure 3

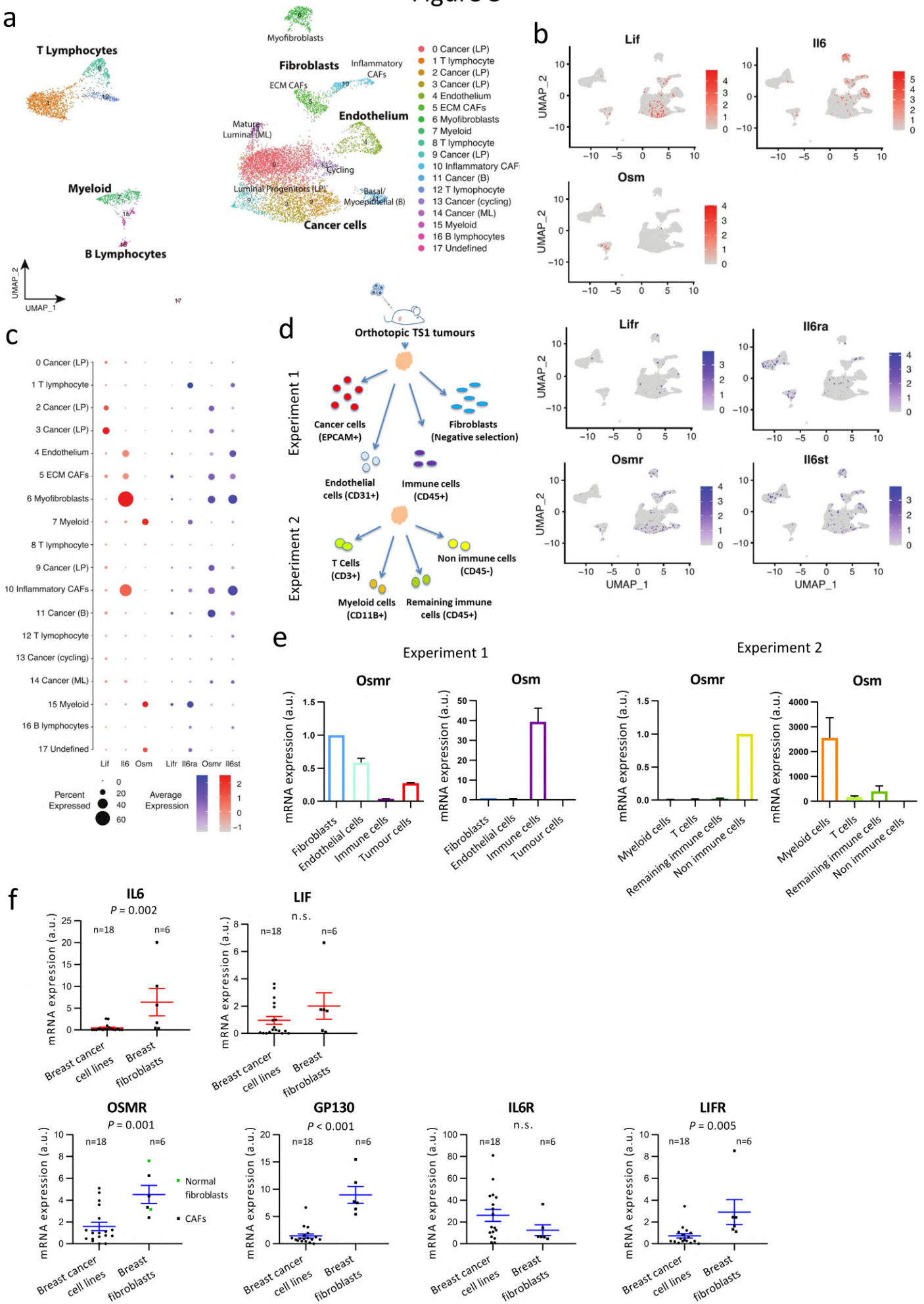
a
T Lymphocytes
Myofibroblasts
Fibroblasts
Inflammatory CAFs
ECM CAFs
Endothelium
Mature Luminal (ML)
Cycling
Luminal Progenitors (LP)
Basal/ Myoepithelial (B)
Cancer cells
Myeloid
B Lymphocytes
UMAP_2
UMAP_1
0 Cancer (LP)
1 T lymphocyte
2 Cancer (LP)
3 Cancer (LP)
4 Endothelium
5 ECM CAFs
6 Myofibroblasts
7 Myeloid
8 T lymphocyte
9 Cancer (LP)
10 Inflammatory CAFs
11 Cancer (B)
12 T lymophocyte
13 Cancer (cycling)
14 Cancer (ML)
15 Myeloid
16 B lymphocytes
17 Undefined
b
Lif
Il6
Osm
Lifr
Il6ra
Osmr
Il6st
UMAP_2
UMAP_1
c
0 Cancer (LP)
1 T lymphocyte
2 Cancer (LP)
3 Cancer (LP)
4 Endothelium
5 ECM CAFs
6 Myofibroblasts
7 Myeloid
8 T lymphocyte
9 Cancer (LP)
10 Inflammatory CAFs
11 Cancer (B)
12 T lymophocyte
13 Cancer (cycling)
14 Cancer (ML)
15 Myeloid
16 B lymphocytes
17 Undefined
Lif Il6 Osm Lifr Il6ra Osmr Il6st
Percent Expressed
0 20 40 60
Average Expression
2 1 0 −1
d
Orthotopic TS1 tumours
Experiment 1
Cancer cells (EPCAM+)
Fibroblasts (Negative selection)
Endothelial cells (CD31+)
Immune cells (CD45+)
Experiment 2
T Cells (CD3+)
Non immune cells (CD45-)
Myeloid cells (CD11B+)
Remaining immune cells (CD45+)
e
Experiment 1
Experiment 2
Osmr
Osm
mRNA expression (a.u.)
Fibroblasts
Endothelial cells
Immune cells
Tumour cells
Myeloid cells
T cells
Remaining immune cells
Non immune cells
f
IL6
P = 0.002
LIF
n.s.
OSMR
P = 0.001
GP130
P < 0.001
IL6R
n.s.
LIFR
P = 0.005
n=18
n=6
mRNA expression (a.u.)
Breast cancer cell lines
Breast fibroblasts
Normal fibroblasts
CAFs

# Figure 4

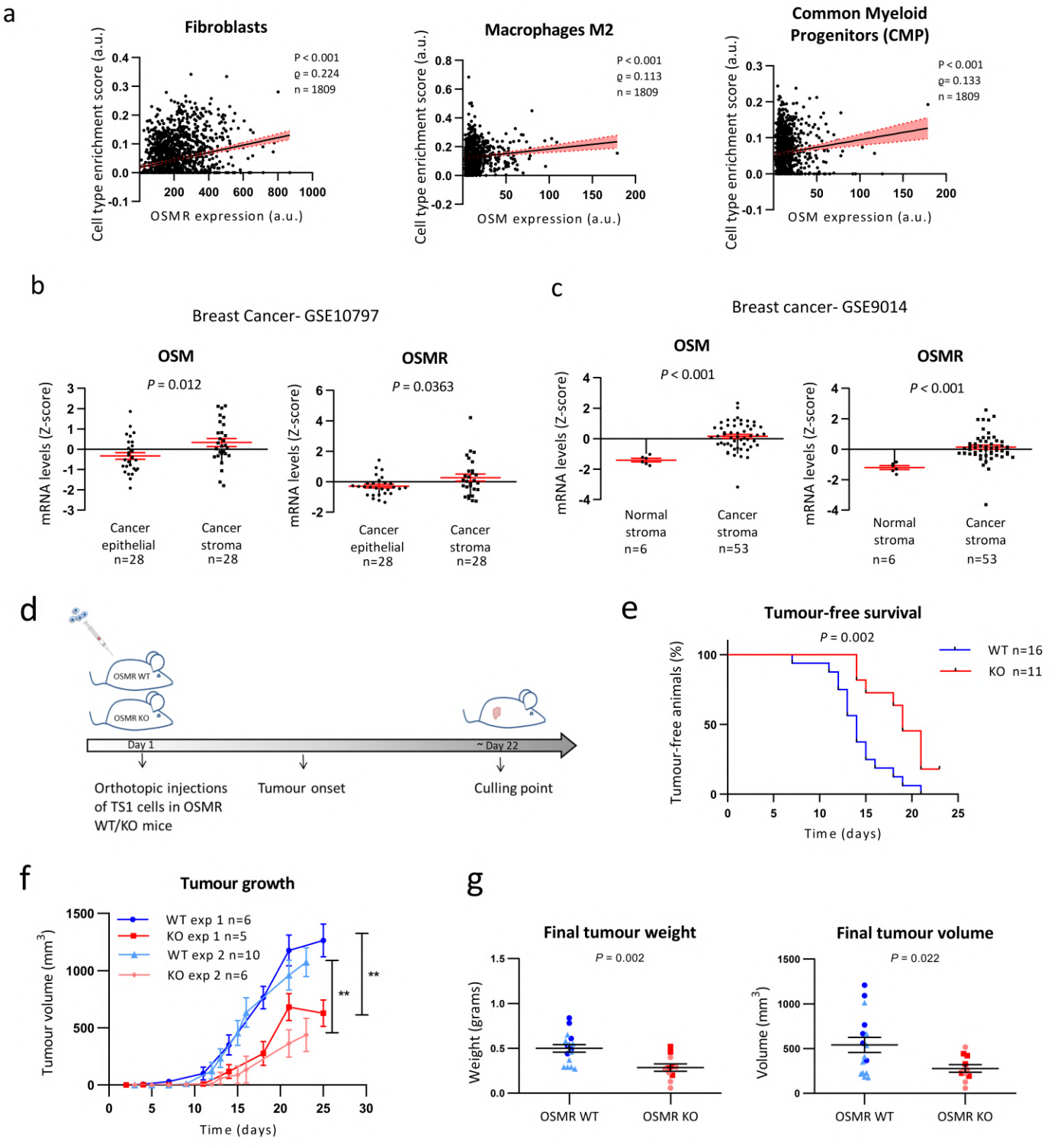
a
Fibroblasts
Cell type enrichment score (a.u.)
OSMR expression (a.u.)
P < 0.001
ϱ = 0.224
n = 1809
Macrophages M2
OSM expression (a.u.)
P < 0.001
ϱ = 0.113
n = 1809
Common Myeloid Progenitors (CMP)
OSM expression (a.u.)
P < 0.001
ϱ= 0.133
n = 1809
b
Breast Cancer- GSE10797
OSM
P = 0.012
mRNA levels (Z-score)
Cancer epithelial n=28
Cancer stroma n=28
OSMR
P = 0.0363
c
Breast cancer- GSE9014
OSM
P < 0.001
Normal stroma n=6
Cancer stroma n=53
OSMR
P < 0.001
d
OSMR WT
OSMR KO
Day 1
~ Day 22
Orthotopic injections of TS1 cells in OSMR WT/KO mice
Tumour onset
Culling point
e
Tumour-free survival
P = 0.002
WT n=16
KO n=11
Tumour-free animals (%)
Time (days)
f
Tumour growth
WT exp 1 n=6
KO exp 1 n=5
WT exp 2 n=10
KO exp 2 n=6
Tumour volume (mm3)
Time (days)
g
Final tumour weight
P = 0.002
Weight (grams)
OSMR WT
OSMR KO
Final tumour volume
P = 0.022
Volume (mm3)

# Figure 5

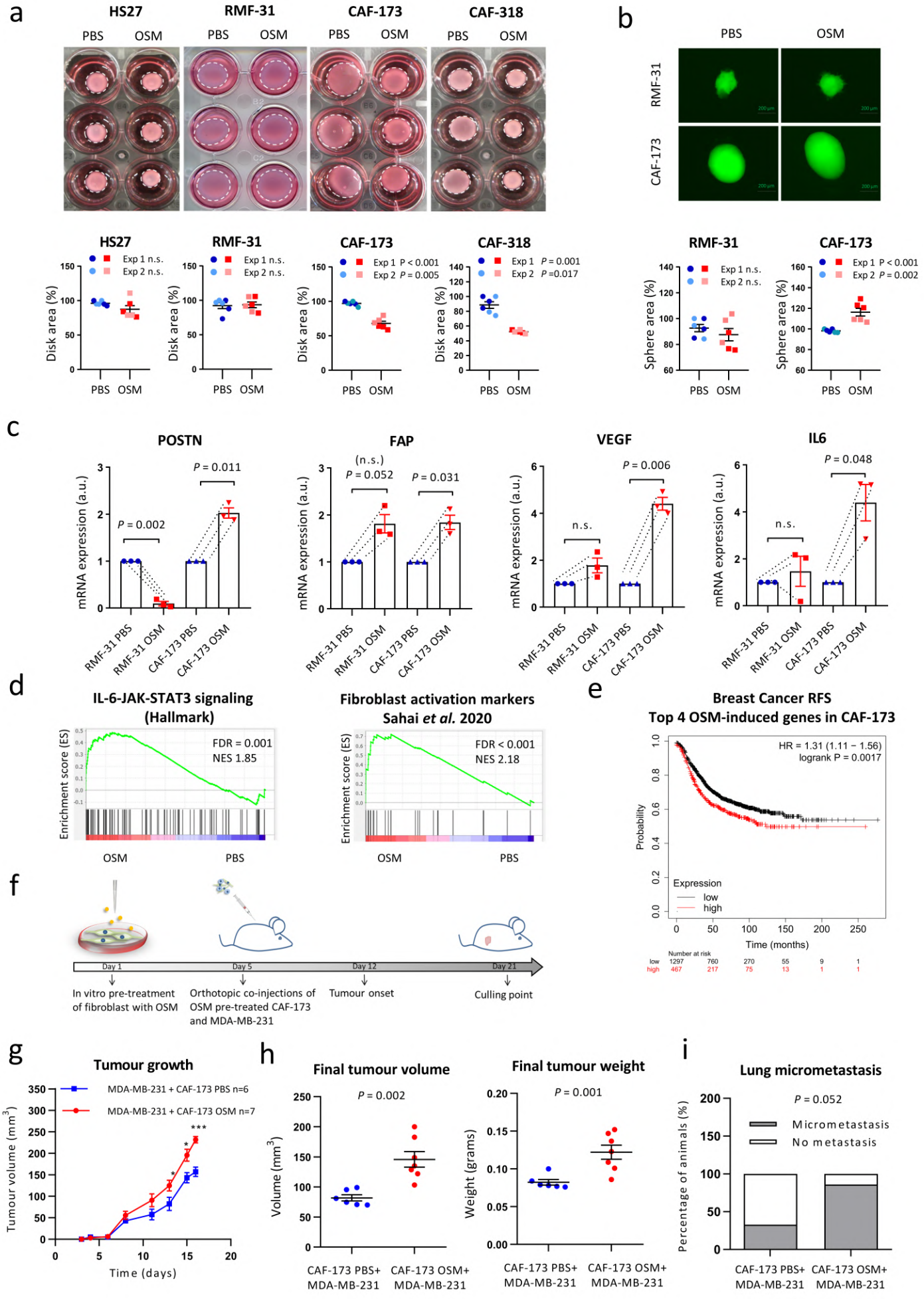
a
HS27
RMF-31
CAF-173
CAF-318
PBS
OSM
Disk area (%)
Exp 1 n.s.
Exp 2 n.s.
Exp 1 P < 0.001
Exp 2 P = 0.005
Exp 1 P = 0.001
Exp 2 P =0.017
b
RMF-31
CAF-173
Sphere area (%)
Exp 1 n.s.
Exp 2 n.s.
Exp 1 P < 0.001
Exp 2 P = 0.002
c
POSTN
FAP
VEGF
IL6
mRNA expression (a.u.)
P = 0.002
P = 0.011
(n.s.)
P = 0.052
P = 0.031
n.s.
P = 0.006
n.s.
P = 0.048
RMF-31 PBS
RMF-31 OSM
CAF-173 PBS
CAF-173 OSM
d
IL-6-JAK-STAT3 signaling (Hallmark)
FDR = 0.001
NES 1.85
Fibroblast activation markers Sahai et al. 2020
FDR < 0.001
NES 2.18
Enrichment score (ES)
OSM
PBS
e
Breast Cancer RFS
Top 4 OSM-induced genes in CAF-173
HR = 1.31 (1.11 − 1.56)
logrank P = 0.0017
Probability
Expression
low
high
Time (months)
Number at risk
low 1297 760 270 55 9 1
high 467 217 75 13 1 1
f
Day 1
Day 5
Day 12
Day 21
In vitro pre-treatment of fibroblast with OSM
Orthotopic co-injections of OSM pre-treated CAF-173 and MDA-MB-231
Tumour onset
Culling point
g
Tumour growth
MDA-MB-231 + CAF-173 PBS n=6
MDA-MB-231 + CAF-173 OSM n=7
Tumour volume (mm3)
Time (days)
h
Final tumour volume
P = 0.002
Volume (mm3)
Final tumour weight
P = 0.001
Weight (grams)
CAF-173 PBS+ MDA-MB-231
CAF-173 OSM+ MDA-MB-231
i
Lung micrometastasis
P = 0.052
Micrometastasis
No metastasis
Percentage of animals (%)

# Figure 6

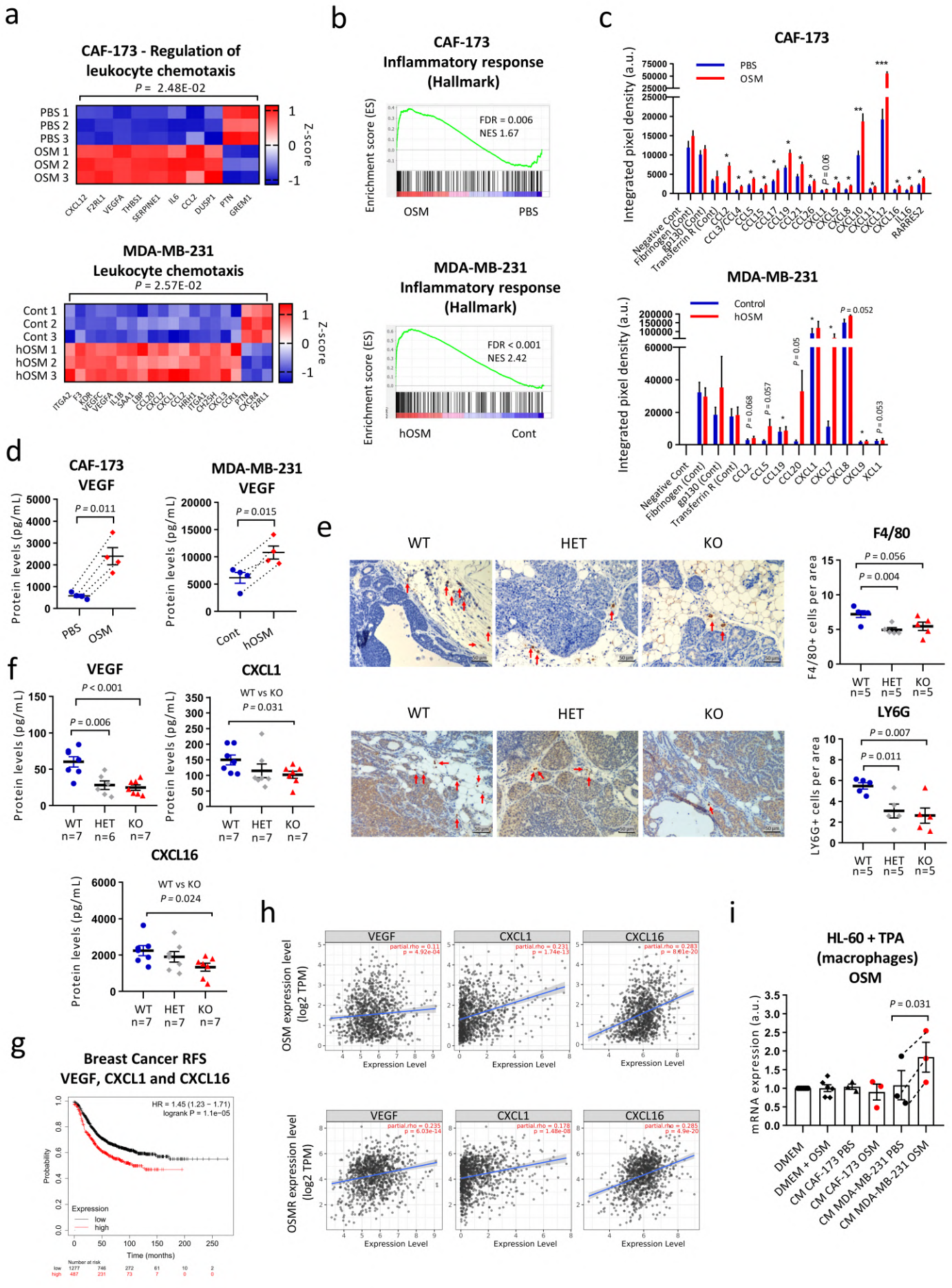
a
CAF-173 - Regulation of leukocyte chemotaxis
P = 2.48E-02
PBS 1
PBS 2
PBS 3
OSM 1
OSM 2
OSM 3
Z-score
CXCL12 F2RL1 VEGFA THBS1 SERPINE1 IL6 CCL2 DUSP1 PTN GREM1
MDA-MB-231
Leukocyte chemotaxis
P = 2.57E-02
Cont 1
Cont 2
Cont 3
hOSM 1
hOSM 2
hOSM 3
ITGA2 F3 KDR VEGFC VEGFA IL1B SAA1 IBP CCL20 CXCL2 CXCL1 CCL2 HRH1 ITGA5 CH25H CXCL3 CCR1 PTN CXCR4 F2RL1
b
CAF-173
Inflammatory response (Hallmark)
FDR = 0.006
NES 1.67
Enrichment score (ES)
OSM
PBS
MDA-MB-231
Inflammatory response (Hallmark)
FDR < 0.001
NES 2.42
hOSM
Cont
c
CAF-173
PBS
OSM
Integrated pixel density (a.u.)
P = 0.06
Negative Cont
Fibrinogen (Cont)
gp130 (Cont)
Transferrin R (Cont)
CCL2 CCL3/CCL4 CCL5 CCL15 CCL17 CCL19 CCL21 CCL26 CXCL1 CXCL5 CXCL8 CXCL10 CXCL11 CXCL12 CXCL16 IL6 RARRES2
MDA-MB-231
Control
hOSM
P = 0.052
P = 0.05
P = 0.057
P = 0.068
P = 0.053
CCL2 CCL5 CCL19 CCL20 CXCL1 CXCL7 CXCL8 CXCL9 XCL1
d
CAF-173
VEGF
P = 0.011
Protein levels (pg/mL)
PBS
OSM
MDA-MB-231
VEGF
P = 0.015
Cont
hOSM
e
WT
HET
KO
F4/80
P = 0.056
P = 0.004
F4/80+ cells per area
WT n=5
HET n=5
KO n=5
LY6G
P = 0.007
P = 0.011
LY6G+ cells per area
f
VEGF
P < 0.001
P = 0.006
CXCL1
WT vs KO
P = 0.031
CXCL16
WT vs KO
P = 0.024
WT n=7
HET n=6
KO n=7
g
Breast Cancer RFS
VEGF, CXCL1 and CXCL16
HR = 1.45 (1.23 – 1.71)
logrank P = 1.1e−05
Probability
Expression
low
high
Time (months)
Number at risk
h
VEGF
CXCL1
CXCL16
OSM expression level (log2 TPM)
OSMR expression level (log2 TPM)
Expression Level
i
HL-60 + TPA (macrophages)
OSM
P = 0.031
mRNA expression (a.u.)
DMEM
DMEM + OSM
CM CAF-173 PBS
CM CAF-173 OSM
CM MDA-MB-231 PBS
CM MDA-MB-231 OSM

Figure 7

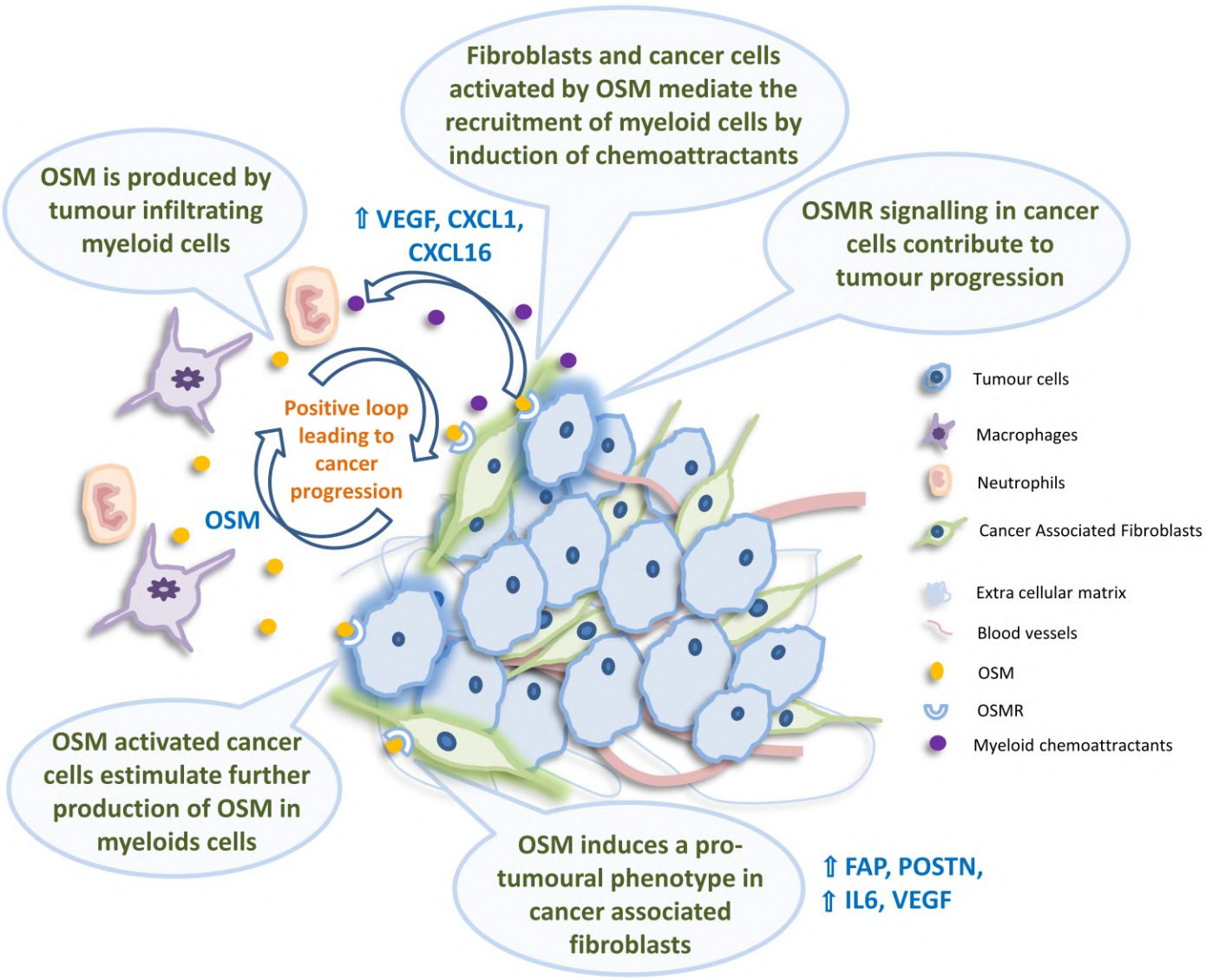
Fibroblasts and cancer cells activated by OSM mediate the recruitment of myeloid cells by induction of chemoattractants
OSM is produced by tumour infiltrating myeloid cells
⇧ VEGF, CXCL1, CXCL16
OSMR signalling in cancer cells contribute to tumour progression
Positive loop leading to cancer progression
OSM
Tumour cells
Macrophages
Neutrophils
Cancer Associated Fibroblasts
Extra cellular matrix
Blood vessels
OSM
OSMR
Myeloid chemoattractants
OSM activated cancer cells estimulate further production of OSM in myeloids cells
OSM induces a pro-tumoural phenotype in cancer associated fibroblasts
⇧ FAP, POSTN, ⇧ IL6, VEGF